mutant genotypes possessing the S108N mutation became more frequent in the late 1990s than in the early 1990s. SP had been used as a secondary treatment for CQ-resistant falciparum malaria in limited African countries before the mid-1990s [5], but was widely deployed in many African countries following the first official introduction of SP as the first-line treatment for uncomplicated malaria in Malawi in 1993. Therefore it seems likely that increased Pyr pressure may have led to the increased prevalence of dhfr genotypes with the S108N mutation, and the observed reduction in the three Pyr-sensitive genotypes (NRSI, ICSI, IRSI) and wild-type (NCSI) in Africa.

This study also showed that the dhfr triple mutant (IRNI), a highly Pyr-resistant genotype, was already present in Central and West Africa in the early 1990s; Nigeria in 1991, Uganda in 1992, and Mali in 1993. The earliest appearance of the IRNI genotype, known to date, was in 1988 in Kenya [22], and this genotype was shown to have been introduced from Southeast Asia. Most of the IRNI genotype currently prevalent in Africa has been generated from this migrated resistant parasite lineage [14,18,19,28], which arrived in East Africa then rapidly moved westwards. Thus, the identification of the IRNI genotype in Nigeria in 1991 supports the idea that the Southeast Asian resistant parasite had already migrated into Central/West Africa in the early 1990s, during which time treatment with Pyr was not common in Africa. However, this idea needs to be confirmed because migration of this type from Southeast Asia cannot be substantiated without the assessment of microsatellite haplotypes flanking dhfr [18,19]. Indeed, an indigenous origin of the same triple mutant (IRNI) genotype, having microsatellite haplotypes distinctive from the Southeast Asian haplotypes, has recently been shown in Cameroon [29] and Kenya [14,30]. In the present study, unfortunately, it was not feasible to determine the lineage of the resistant parasite with the triple mutant (IRNI) genotype, as sufficient amounts of DNA required to determine the microsatellite haplotypes could not be recovered from the Giemsa-stained thin blood smears. However, the recently discovered indigenous African parasite lineage was observed in low frequency compared to the Southeast Asian parasite lineage [14,29]. Hence, it seems likely that the Southeast Asian parasite lineage had already migrated to Africa before SP was widely used in Africa, and subsequently spread across the continent after the increased use of SP.

The highest Pyr-resistant dhfr genotype, quadruple mutant (IRNL), was not identified in the present sample set. Consistently, the earliest record of the appearance of IRNL genotype in Africa was in 1999 from Uganda [31] – in 2000 from Tanzania [32]. However, the prevalence of the IRNL genotype is notably still low in many endemic countries in Africa [30] in spite of the intense usage of SP as a first-line therapy [33]. This is in sharp contrast to a high prevalence of the IRNL genotype in Indochina, where the genotype has remarkably increased after the initial identification in the late 1980s [33,34]. Many factors appear to be associated with the observed difference of the prevalence of the IRNL genotype between Africa and Indochina. One factor could be a level of acquired immunity against falciparum malaria. In many endemic areas in Africa, adults acquire semi-immunity after repeated infections. In those individuals SP is considered to be effective to not only Pyr-sensitive parasites but also Pyr-resistant parasites. Importantly, the IRNL genotype is reportedly not associated with SP treatment failure or in vivo resistance in individuals who have high levels of immunity to malaria [33,35]. It is thus suggested that the IRNL genotype has not been strongly selected for by SP pressure in semi-immune African adults, and consequently the genotype has not expanded in Africa. Other factors that have retarded the expansion of the IRNL genotype in Africa cannot be excluded, and this issue needs to be clarified in the near future.

This study is the first to report the occurrence of the CVIET CQ-resistant pfcrt genotype as early as 1984 in Nigeria. Previously, the oldest identification of the pfcrt mutant genotype was in 1989 in East Africa [21] and in 1992 in West Africa [36]. This strongly suggests that CQ resistance, which first arrived in East Africa from Southeast Asia, had already spread to West Africa by 1984. Around that time, however, CQ efficacy was satisfactory in the countries of western Africa, and several in vivo tolerance and resistance cases were reported only in non-immune individuals [37-39]. Acquired immunity against malaria in individuals in highly endemic areas in Africa may have strengthened the efficacy of CQ against the CQ-resistant parasites [6,7] and probably masked the appearance of clinical CQ resistance.

In contrast to the mainland of Africa, where resistance to CQ and Pyr is widely spread, CQ and Pyr are still effective in Madagascar and Comoros in the south-western Indian Ocean [40]. A recent report has shown that Pyr resistant genotypes found in Madagascar were introduced from

Comoros [41]. Unfortunately, the present sample set included only one sample from Madagascar, and thus it is difficult to infer when and from where drug resistant genotype was introduced to Madagascar and Comoros islands. Further molecular surveys of samples from African countries including Madagascar and Comoros are required for better understanding of the evolutionary history of drug resistance in the continent.

Conclusions

The present study used archive blood samples to reveal new aspects of the evolutionary history of Plasmodium falciparum resistance to Pyr and CQ in Africa. Pyr-sensitive mutant genotypes lacking the S108N mutation were frequently observed in the 1980s but were drastically reduced in the late 1990s, and instead, the frequency of highly Pyr-resistant genotypes (double and triple mutants) considerably increased after the mid-1990s. In addition, the CQ-resistant pfcrt genotype, CVIET, was identified as early as 1984 in West Africa. Further molecular epidemiological investigations using archive samples from diverse endemic areas would lead to a better understanding of the evolutionary history of drug resistance of P. falciparum.

Competing interests

The authors declare that they have no competing interests.

Authors' contributions

YSN conducted the genotyping, data collection, and prepared the manuscript. KT participated in the design of the study, and provided critical input on the manuscript. TM assisted with the population genetic analysis, and contributed helpful input to the manuscript. All authors have read and approved the final version of the manuscript.

Acknowledgements

We thank Eiko Nakasone for technical support. We also acknowledge the staff who participated in sample collection for the national surveillance system. This work was supported by a Grant-in-Aid from the Ministry of Health, Labour and Welfare of Japan (grant H20–Shinkou-ippan-013), a grant for Research on Emerging and Re-emerging Infectious Diseases from the Ministry of Health, Labour and Welfare of Japan (H23-Shinko-Ippan-014), and from the Ministry of Education, Culture, Sports, Science, and Technology of Japan (22406012, 23590498, 23659211).

References

1. Campbell CC, Chin W, Collins WE, Teutsch SM, Moss DM: Chloroquine-resistant Plasmodium falciparum from East Africa: cultivation and drug sensitivity of the Tanzanian I/CDC strain from an American tourist. Lancet 1979, 2:1151–1154.

2. Fogh S, Jepsen S, Effersoe P: Chloroquine-resistant Plasmodium falciparum malaria in Kenya. Trans R Soc Trop Med Hyg 1979, 73:228–229.

3. Clyde DF, Shute GT: Resistance of Plasmodium falciparum in Tanganyika to pyrimethamine administered at weekly intervals. Trans R Soc Trop Med Hyg 1957, 51:505–513.

4. Naidoo I, Roper C: Following the path of most resistance: dhps K540E dispersal in African Plasmodium falciparum. Trends Parasitol 2010, 26:447–456.

5. Talisuna AO, Bloland P, D'Alessandro U: History, dynamics, and public health importance of malaria parasite resistance. Clin Microbiol Rev 2004, 17:235–254.

6. Gatton ML, Martin LB, Cheng Q: Evolution of resistance to sulfadoxine-pyrimethamine in Plasmodium falciparum. Antimicrob Agents Chemother 2004, 48:2116–2123.

7. Hastings IM, Korenromp EL, Bloland PB: The anatomy of a malaria disaster: drug policy choice and mortality in African children. Lancet Infect Dis 2007, 7:739–748.

8. Fidock DA, Nomura T, Talley AK, Cooper RA, Dzekunov SM, Ferdig MT, Ursos LM, Sidhu AB, Naude B, Deitsch KW, et al: Mutations in the P. falciparum digestive vacuole transmembrane protein PfCRT and evidence for their role in chloroquine resistance. Mol Cell 2000, 6:861–871.

9. Cooper RA, Ferdig MT, Su XZ, Ursos LM, Mu J, Nomura T, Fujioka H, Fidock DA, Roepe PD, Wellems TE: Alternative mutations at position 76 of the vacuolar transmembrane protein PfCRT are associated with chloroquine resistance and unique stereospecific quinine and quinidine responses in Plasmodium falciparum. Mol Pharmacol 2002, 61:35–42.

10. Peterson DS, Walliker D, Wellems TE: Evidence that a point mutation in dihydrofolate reductase-thymidylate synthase confers resistance to pyrimethamine in falciparum malaria. Proc Natl Acad Sci U S A 1988, 85:9114–9118.

11. Sirawaraporn W, Sathitkul T, Sirawaraporn R, Yuthavong Y, Santi DV: Antifolate-resistant mutants of Plasmodium falciparum dihydrofolate reductase. Proc Natl Acad Sci U S A 1997, 94:1124–1129.

12. Brown KM, Costanzo MS, Xu W, Roy S, Lozovsky ER, Hartl DL: Compensatory mutations restore fitness during the evolution of dihydrofolate reductase. Mol Biol Evol 2010, 27:2682–2690.

13. Lozovsky ER, Chookajorn T, Brown KM, Imwong M, Shaw PJ, Kamchonwongpaisan S, Neafsey DE, Weinreich DM, Hartl DL: Stepwise acquisition of pyrimethamine resistance in the malaria parasite. Proc Natl Acad Sci U S A 2009, 106:12025–12030.

14. Mita T, Tanabe K, Takahashi N, Culleton R, Ndounga M, Dzodzomenyo M, Akhwale WS, Kaneko A, Kobayakawa T: Indigenous evolution of Plasmodium falciparum pyrimethamine resistance multiple times in Africa. J Antimicrob Chemother 2009, 63:252–255.

15. Chen N, Russell B, Staley J, Kotecka B, Nasveld P, Cheng Q: Sequence polymorphisms in pfcrt are strongly associated with chloroquine resistance in Plasmodium falciparum. J Infect Dis 2001, 183:1543–1545.

16. Wellems TE, Hayton K, Fairhurst RM: The impact of malaria parasitism: from corpuscles to communities. Journal Clinical Investigation 2009, 119:2496–2505.

17. Wootton JC, Feng X, Ferdig MT, Cooper RA, Mu J, Baruch DI, Magill AJ, Su XZ: Genetic diversity and chloroquine selective sweeps in Plasmodium falciparum. Nature 2002, 418:320–323.

18. Maiga O, Djimde AA, Hubert V, Renard E, Aubouy A, Kironde F, Nsimba B, Koram K, Doumbo OK, Le Bras J, Clain J: A shared Asian origin of the triple-mutant dhfr allele in Plasmodium falciparum from sites across Africa. J Infect Dis 2007, 196:165–172.

19. Roper C, Pearce R, Nair S, Sharp B, Nosten F, Anderson T: Intercontinental spread of pyrimethamine-resistant malaria. Science 2004, 305:1124.

20. Cowman AF, Morry MJ, Biggs BA, Cross GA, Foote SJ: Amino acid changes linked to pyrimethamine resistance in the dihydrofolate reductase-thymidylate synthase gene of Plasmodium falciparum. Proc Natl Acad Sci U S A 1988, 85:9109–9113.

21. Babiker HA, Pringle SJ, Abdel-Muhsin A, Mackinnon M, Hunt P, Walliker D: High-level chloroquine resistance in Sudanese isolates of Plasmodium falciparum is associated with mutations in the chloroquine resistance transporter gene pfcrt and the multidrug resistance Gene pfmdr1. J Infect Dis 2001, 183:1535–1538.

22. Certain LK, Briceno M, Kiara SM, Nzila AM, Watkins WM, Sibley CH: Characteristics of Plasmodium falciparum dhfr haplotypes that confer pyrimethamine resistance, Kilifi, Kenya, 1987–2006. J Infect Dis 2008, 197:1743–1751.

23. Saito-Nakano Y, Tanabe K, Kamei K, Iwagami M, Komaki-Yasuda K, Kawazu S, Kano S, Ohmae H, Endo T: Genetic evidence for Plasmodium falciparum resistance to chloroquine and pyrimethamine in Indochina and the Western Pacific between 1984 and 1998. Am J Trop Med Hyg 2008, 79:613–619.

24. Cnops L, Van Esbroeck M, Bottieau E, Jacobs J: Giemsa-stained thick blood films as a source of DNA for Plasmodium species-specific real-time PCR. Malar J 2010, 9:370.

25. Volpini AC, Marques MJ, Lopes dos Santos S, Machado-Coelho GL, Mayrink W, Romanha AJ: Leishmania identification by PCR of Giemsa-stained lesion imprint slides stored for up to 36 years. Clin Microbiol Infect 2006, 12:815–818.

26. Mita T, Tanabe K, Kita K: Spread and evolution of Plasmodium falciparum drug resistance. Parasitol Int 2009, 58:201–209.

27. Ferlan JT, Mookherjee S, Okezie IN, Fulgence L, Sibley CH: Mutagenesis of dihydrofolate reductase from Plasmodium falciparum: analysis in Saccharomyces cerevisiae of triple mutant alleles resistant to pyrimethamine or WR99210. Mol Biochem Parasitol 2001, 113:139–150.

28. McCollum AM, Mueller K, Villegas L, Udhayakumar V, Escalante AA: Common origin and fixation of Plasmodium falciparum dhfr and dhps mutations associated with sulfadoxine-pyrimethamine resistance in a low-transmission area in South America. Antimicrob Agents Chemother 2007, 51:2085–2091.

29. McCollum AM, Basco LK, Tahar R, Udhayakumar V, Escalante AA: Hitchhiking and selective sweeps of Plasmodium falciparum sulfadoxine and pyrimethamine resistance alleles in a population from central Africa. Antimicrob Agents Chemother 2008, 52:4089–4097.

30. McCollum AM, Poe AC, Hamel M, Huber C, Zhou Z, Shi YP, Ouma P, Vulule J, Bloland P, Slutsker L, et al: Antifolate resistance in Plasmodium falciparum: multiple origins and identification of novel dhfr alleles. J Infect Dis 2006, 194:189–197.

31. Alker AP, Mwapasa V, Purfield A, Rogerson SJ, Molyneux ME, Kamwendo DD, Tadesse E, Chaluluka E, Meshnick SR: Mutations associated with sulfadoxine-pyrimethamine and chlorproguanil resistance in Plasmodium falciparum isolates from Blantyre, Malawi. Antimicrob Agents Chemother 2005, 49:3919–3921.

32. Hastings MD, Bates SJ, Blackstone EA, Monks SM, Mutabingwa TK, Sibley CH: Highly pyrimethamine-resistant alleles of dihydrofolate reductase in isolates of Plasmodium falciparum from Tanzania. Trans R Soc Trop Med Hyg 2002, 96:674–676.

33. Hyde JE: Antifolate resistance in Africa and the 164-dollar question. Trans R Soc Trop Med Hyg 2008, 102:301–303.

34. Foote SJ, Galatis D, Cowman AF: Amino acids in the dihydrofolate reductase-thymidylate synthase gene of Plasmodium falciparum involved in cycloguanil resistance differ from those involved in pyrimethamine resistance. Proc Natl Acad Sci U S A 1990, 87:3014–3017.

35. Krudsood S, Imwong M, Wilairatana P, Pukrittayakamee S, Nonprasert A, Snounou G, White NJ, Looareesuwan S: Artesunate-dapsone-proguanil treatment of falciparum malaria: genotypic determinants of therapeutic response. Trans R Soc Trop Med Hyg 2005, 99:142–149.

36. Ursing J, Schmidt BA, Lebbad M, Kofoed PE, Dias F, Gil JP, Rombo L: Chloroquine resistant P. falciparum prevalence is low and unchanged between 1990 and 2005 in Guinea-Bissau: an effect of high chloroquine dosage? Infect Genet Evol 2007, 7:555–561.

37. Brandicourt O, Druilhe P, Diouf F, Brasseur P, Turk P, Danis M: Decreased sensitivity to chloroquine and quinine of some Plasmodium falciparum strains from Senegal in September 1984. Am J Trop Med Hyg 1986, 35:717–721.

38. Breman JG, Gayibor A, Roberts JM, Sexton JD, Agbo K, Miller KD, Karsa T, Murphy K: Single-dose chloroquine therapy for Plasmodium falciparum in children in Togo, West Africa. Am J Trop Med Hyg 1987, 36:469–473.

39. Chabasse D, De Gentile L, Ligny C, Le Bras J, Rialland X, Bouchara JP: Chloroquine-resistant Plasmodium falciparum in Mali revealed by congenital malaria. Trans R Soc Trop Med Hyg 1988, 82:547.

40. Andriantsoanirina V, Menard D, Tuseo L, Durand R: History and current status of Plasmodium falciparum antimalarial drug resistance in Madagascar. Scand J Infect Dis 2010, 42:22–32.

41. Andriantsoanirina V, Bouchier C, Tichit M, Jahevitra M, Rabearimanana S, Randrianjafy R, Ratsimbasoa A, Mercereau-Puijalon O, Durand R, Menard D: Origins of the recent emergence of Plasmodium falciparum pyrimethamine resistance alleles in Madagascar. Antimicrob Agents Chemother 2010, 54:2323–2329.

Additional files

Additional_file_1 as PDF
Additional file 1: Table S1. Plasmodium falciparum pfcrt and dhfr genotypes determined in 85 blood smears from Africa between 1984 and 1998. Footnotes: The pfcrt and dhfr genotypes determined are shown for each individual sample. Mutated amino acid residues are underlined. pfcrt, P. falciparum chloroquine-resistance transporter; dhfr, dihydrofolate reductase; nd, not determined.

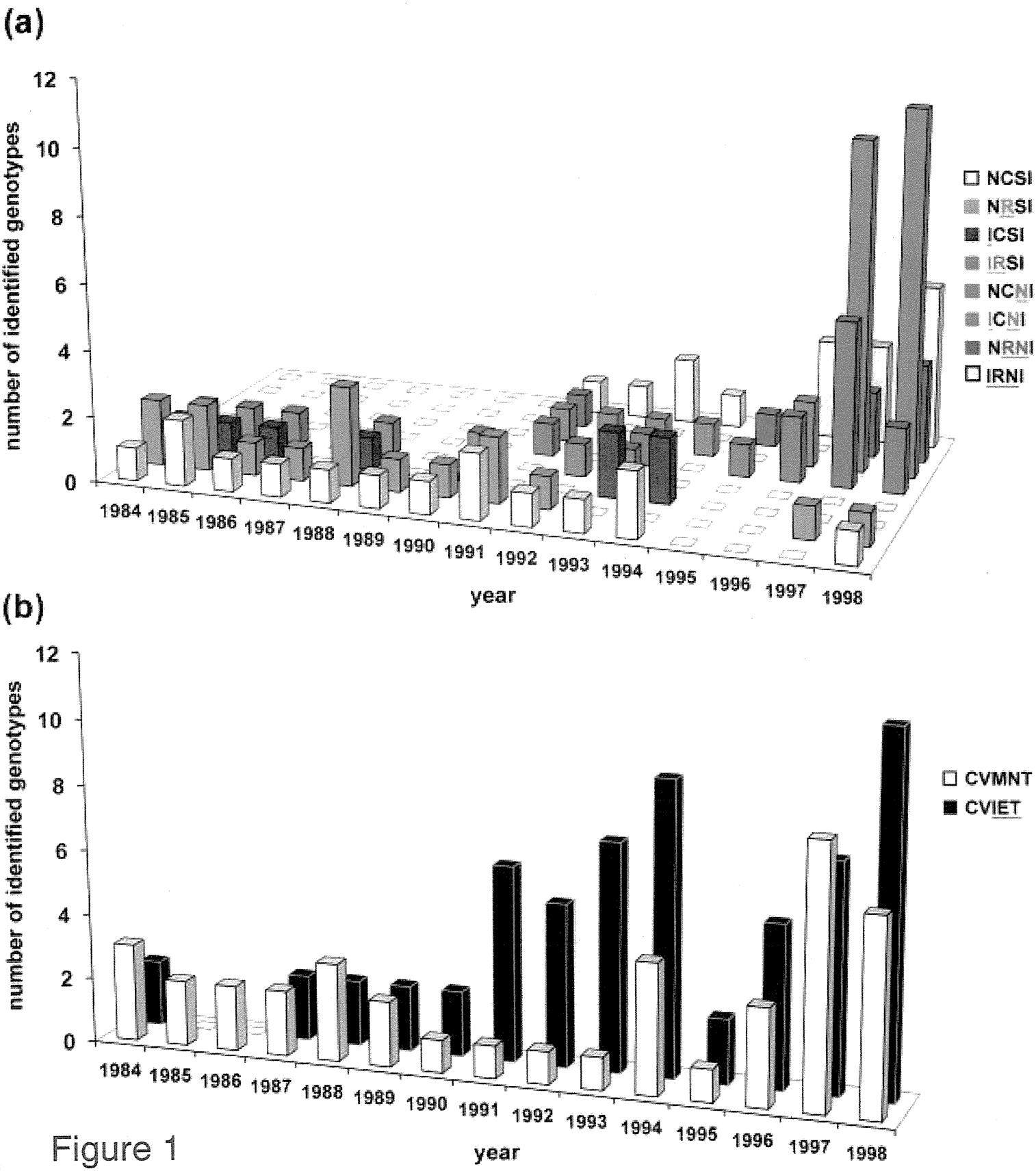
(a)
number of identified genotypes
0
2
4
6
8
10
12
1984
1985
1986
1987
1988
1989
1990
1991
1992
1993
1994
1995
1996
1997
1998
year
NCSI
NRSI
ICSI
IRSI
NCNI
ICNI
NRNI
IRNI
(b)
number of identified genotypes
0
2
4
6
8
10
12
1984
1985
1986
1987
1988
1989
1990
1991
1992
1993
1994
1995
1996
1997
1998
year
CVMNT
CVIET

Figure 1

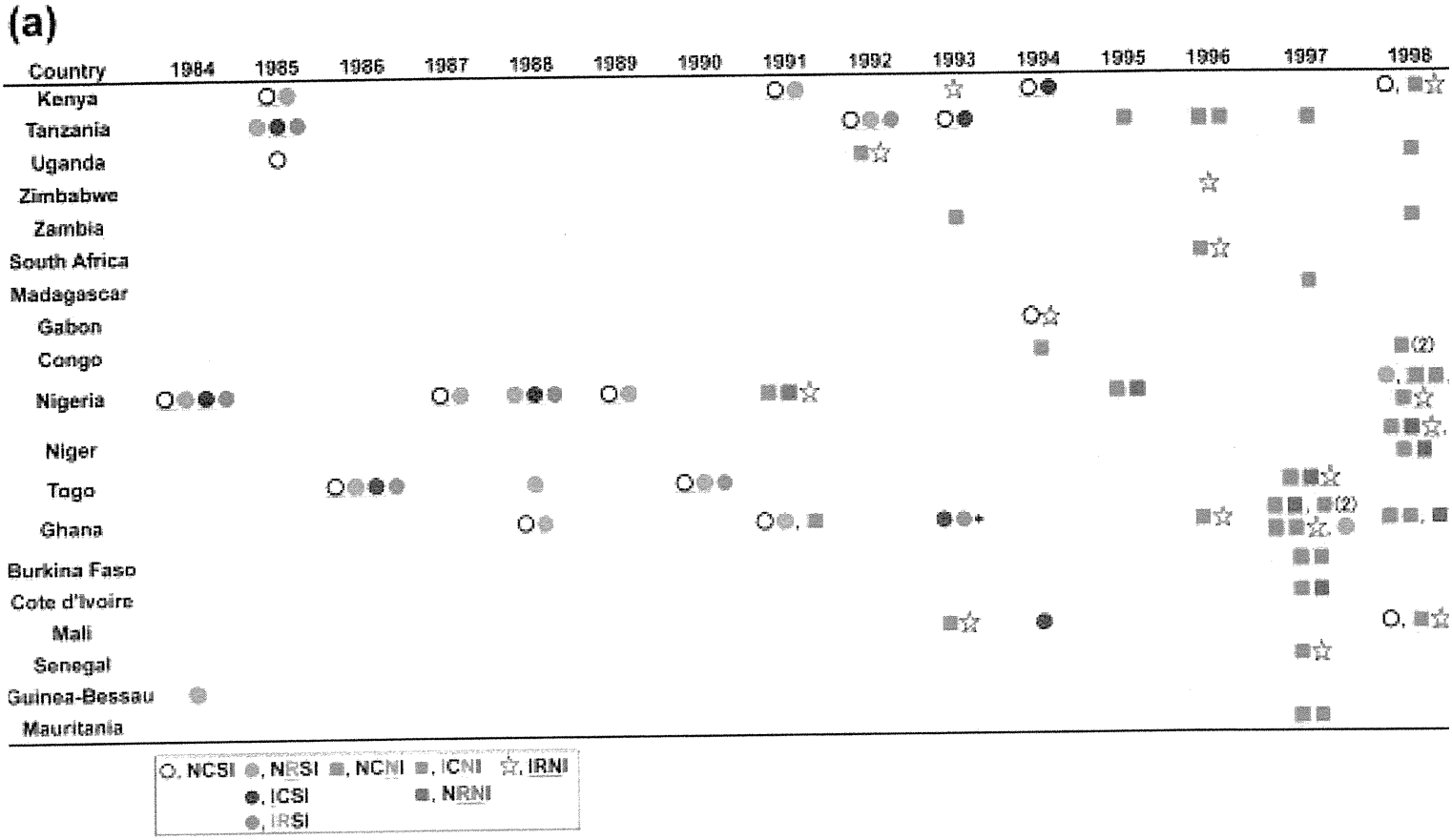
(a)
Country
1984
1985
1986
1987
1988
1989
1990
1991
1992
1993
1994
1995
1996
1997
1998
Kenya
Tanzania
Uganda
Zimbabwe
Zambia
South Africa
Madagascar
Gabon
Congo
Nigeria
Niger
Togo
Ghana
Burkina Faso
Cote d'Ivoire
Mali
Senegal
Guinea-Bessau
Mauritania
○, NCSI ●, NRSI ■, NCNI ■, ICNI ☆, IRNI
●, ICSI ■, NRNI
●, IRSI

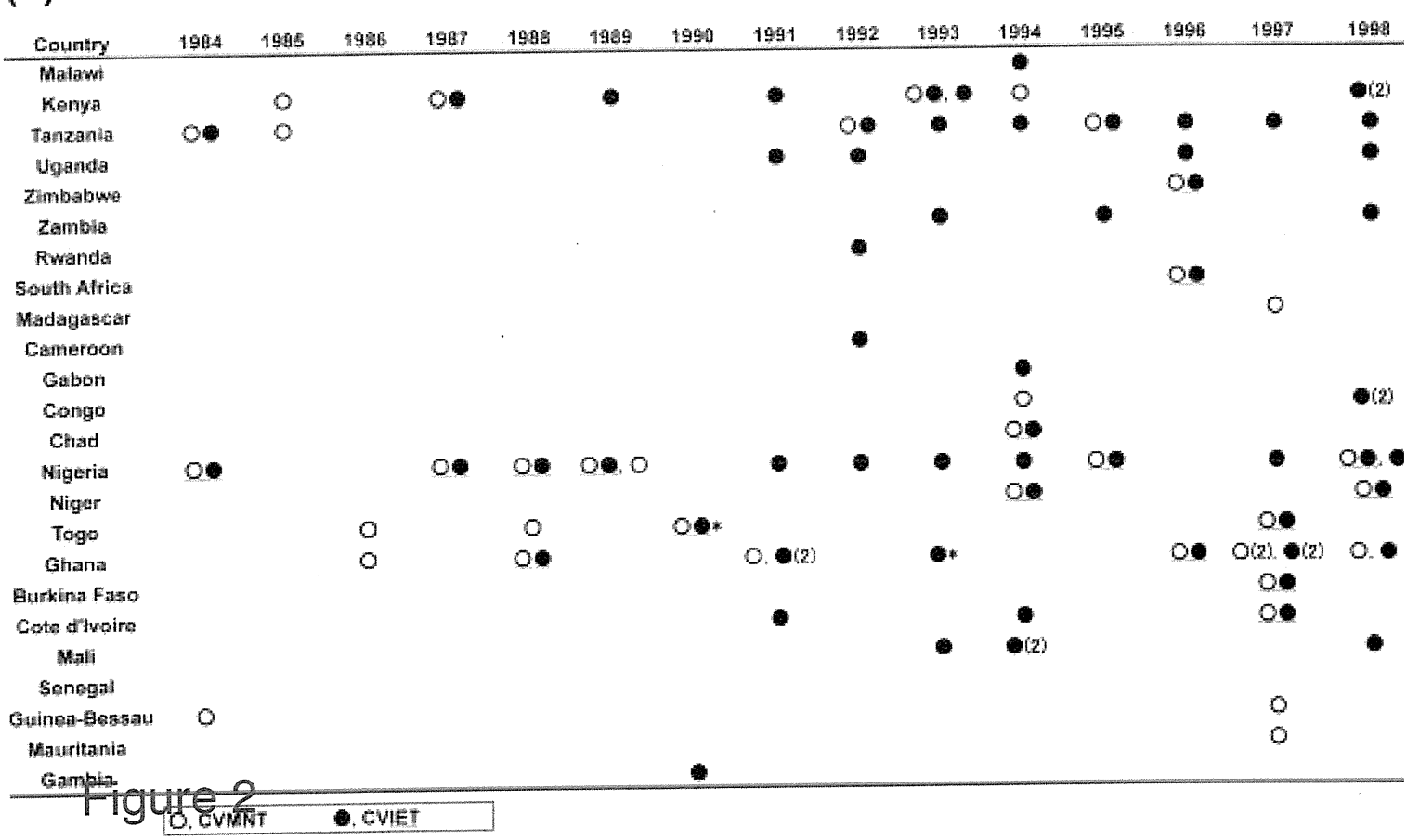
(b)
Country
1984
1985
1986
1987
1988
1989
1990
1991
1992
1993
1994
1995
1996
1997
1998
Malawi
Kenya
Tanzania
Uganda
Zimbabwe
Zambia
Rwanda
South Africa
Madagascar
Cameroon
Gabon
Congo
Chad
Nigeria
Niger
Togo
Ghana
Burkina Faso
Cote d'Ivoire
Mali
Senegal
Guinea-Bessau
Mauritania
Gambia
○, CVMNT ●, CVIET

Figure 2

Additional files provided with this submission:

Additional file 1: Supplementary Table.pdf, 56K
http://www.malariajournal.com/imedia/1588441281610887/supp1.pdf

Published June 13, 2011

JEM

Article

ATF6β is a host cellular target of the *Toxoplasma gondii* virulence factor ROP18

Masahiro Yamamoto,[1,3] Ji Su Ma,[1,3] Christina Mueller,[5] Naganori Kamiyama,[1,3] Hiroyuki Saiga,[1,3] Emi Kubo,[1] Taishi Kimura,[1,3] Toru Okamoto,[4] Megumi Okuyama,[1,3] Hisako Kayama,[1,3] Kisaburo Nagamune,[6] Seiji Takashima,[2] Yoshiharu Matsuura,[4] Dominique Soldati-Favre,[5] and Kiyoshi Takeda[1,3]

[1]Department of Microbiology and Immunology and [2]Department of Cardiovascular Medicine, Graduate School of Medicine; [3]Laboratory of Mucosal Immunology, World Premier International Research Center Immunology Frontier Research Center; and [4]Department of Molecular Virology, Research Institute for Microbial Diseases; Osaka University, Suita, Osaka 565-0871, Japan
[5]Department of Microbiology and Molecular Medicine, University Medical Center, University of Geneva, 1211 Geneva 4, Switzerland
[6]Department of Parasitology, National Institute of Infectious Diseases, Shinjuku-ku, Tokyo 162-8640, Japan

The ROP18 kinase has been identified as a key virulence determinant conferring a high mortality phenotype characteristic of type I *Toxoplasma gondii* strains. This major effector molecule is secreted by the rhoptries into the host cells during invasion; however, the molecular mechanisms by which this kinase exerts its pathogenic action remain poorly understood. In this study, we show that ROP18 targets the host endoplasmic reticulum–bound transcription factor ATF6β. Disruption of the *ROP18* gene severely impairs acute toxoplasmosis by the type I RH strain. Because another virulence factor ROP16 kinase modulates immune responses through its N-terminal portion, we focus on the role of the N terminus of ROP18 in the subversion of host cellular functions. The N-terminal extension of ROP18 contributes to ATF6β-dependent pathogenicity by interacting with ATF6β and destabilizing it. The kinase activity of ROP18 is essential for proteasome-dependent degradation of ATF6β and for parasite virulence. Consistent with a key role for ATF6β in resistance against this intracellular pathogen, ATF6β-deficient mice exhibit a high susceptibility to infection by ROP18-deficient parasites. The results reveal that interference with ATF6β-dependent immune responses is a novel pathogenic mechanism induced by ROP18.

CORRESPONDENCE
Kiyoshi Takeda:
ktakeda@ongene.med.osaka-u.ac.jp

Abbreviations used: BMDC, BM-derived DC; ERAD, ER-associated degradation; GST, glutathione *S*-transferase; HA, hemagglutinin; HFF, human foreskin fibroblast; IRG, immunity-related GTPase; KD, kinase dead; MOI, multiplicity of infection; MPA, mycophenolic acid; PFA, paraformaldehyde; PV, parasitophorous vacuole; PVM, PV membrane; UPR, unfolded protein response; UPRE, UPR element.

Toxoplasma gondii causes life-threatening toxoplasmosis in immunocompromised individuals such as those suffering from AIDS or being treated by chemotherapy (Montoya and Remington, 2008). As a member of the phylum of Apicomplexa, *T. gondii* is an obligate intracellular parasite, defined by the presence of an apical complex including secretory organelles such as rhoptries and micronemes (Joynson and Wreghitt, 2001). During invasion, *T. gondii* delivers numerous effector molecules into the forming parasitophorous vacuole (PV) and the host cytoplasm to co-opt the host cell for growth and survival (Boothroyd and Dubremetz, 2008).

T. gondii is divided into three major lineages (types I, II, and III) in addition to exotic strains (Ajzenberg et al., 2004; Dardé, 2008). Although type II parasites are the most prevailing opportunistic strains, infection with type I strains appears to be responsible for encephalitis in AIDS patients, ocular toxoplasmosis, and congenital hydrocephalus, whereas infection with type III strains seldom results in disease manifestations (Howe and Sibley, 1995; Boothroyd and Grigg, 2002). In terms of the strain-dependent phenotypes, virulence in mice has been well characterized, although the median lethal dose of type II or III parasites ranges from 10^2 to 10^5, and the lethal dose of the most virulent type I strain is one (10^0) parasite (Sibley and Boothroyd, 1992; Sibley and Howe, 1996;

T. Okamoto's present address is The Walter and Eliza Hall Institute of Medical Research, Parkville, Victoria 3052, Australia.

The Rockefeller University Press $30.00
J. Exp. Med. Vol. 208 No. 7 1533-1546
www.jem.org/cgi/doi/10.1084/jem.20101660

Supplemental Material can be found at:
http://jem.rupress.org/content/suppl/2011/06/12/jem.20101660.DC1.html

Published June 13, 2011

Dubremetz, 2007). Previous forward genetic studies, in which types I/II and III were intercrossed to explore genes responsible for virulence, culminated in the identification of *ROP18* as the dominant candidate gene (Saeij et al., 2006; Taylor et al., 2006).

ROP18 is a Ser/Thr kinase related to the ROP2 subfamily, secreted by the rhoptries into the PV and host cytosol. Its action as effector molecule is anticipated to modulate host factors by an as yet unknown mechanism (El Hajj et al., 2006; Taylor et al., 2006; Dubremetz, 2007). Most recently, ROP18 has been shown to target a member of IFN-inducible small GTPases (immunity-related GTPases [IRGs]), Irgb6 (Fentress et al., 2010; Steinfeldt et al., 2010), indicating that interference with the innate function of Irgb6 is a key mechanism by which ROP18 mediates virulence at an early stage after infection. ROP16, another ROP2 subfamily member, was previously identified as virulence determinant, distinguishing how type I/III and II strains activate Stat3/6 during parasite

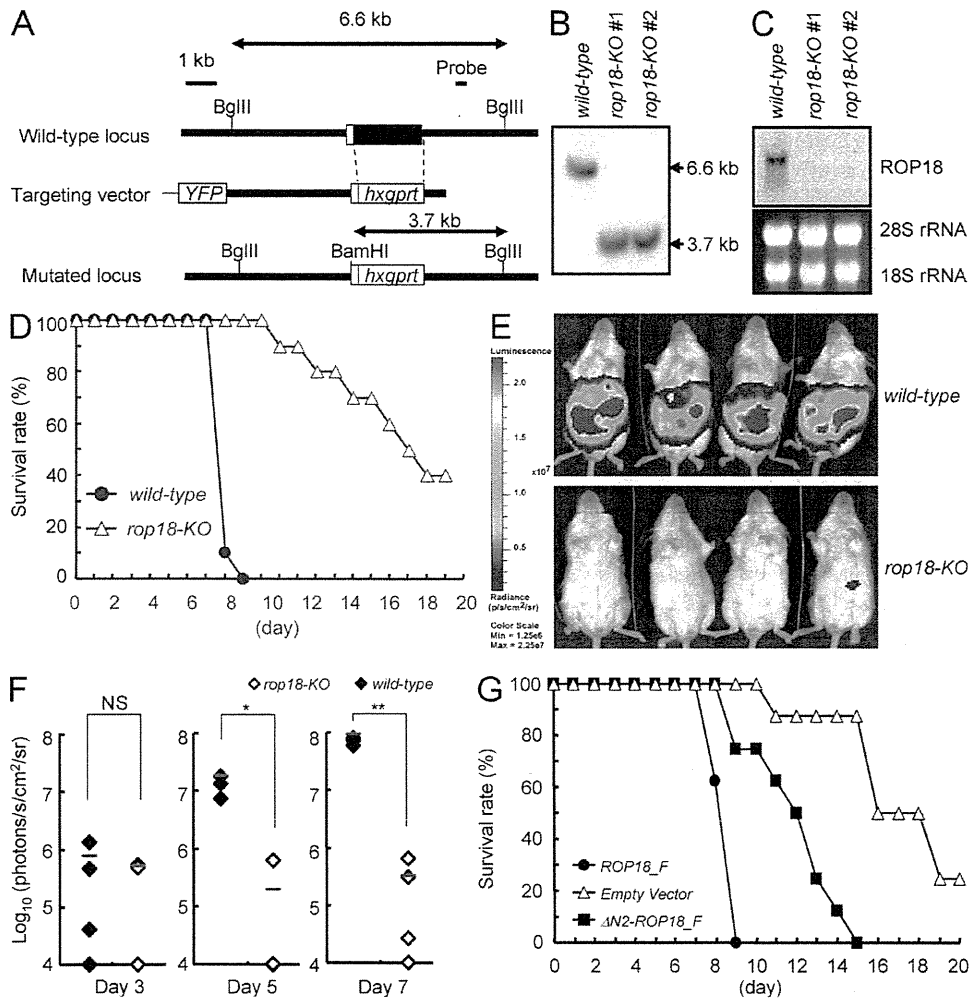

Figure 1. The N terminus of ROP18 is required for acute virulence in type I *T. gondii*. (A) The structure of the *ROP18* gene, the targeting vector, and the predicted disrupted gene. Closed boxes denote the exons. (B) Southern blot analysis of WT or two lines of *rop18-KO* parasites. 30 µg total genomic DNA was extracted from parasites, digested with BglII-BamHI, electrophoresed, and hybridized with the radiolabeled probe indicated in A. Southern blotting yielded a single 6.6-kb band for the WT and a 3.7-kb band for the disrupted locus. (C) Northern blot analysis on 10 µg total parasite RNA separated on a gel, transferred to a nylon membrane, and hybridized with ROP18 probe. The 28S and 18S ribosomal RNA is shown as the loading control (bottom). (D) BALB/c mice ($n = 10$) were infected with 10^3 WT or *rop18-KO* parasites, and the survival rates were monitored for 20 d. (E) BALB/c mice ($n = 4$) were infected with 10^3 WT or *rop18-KO* luciferase-expressing parasites, and the progress of infection was assessed by bioluminescence imaging at day 6 after infection. The color scale indicates photon emission during a 60-s exposure. (F) Total photon emission analysis from BALB/c mice ($n = 4$) infected with 10^3 WT or *rop18-KO* luciferase-expressing parasites at days 3, 5, or 7 after infection. Abdominal photon emission was assessed during a 60-s exposure. The red bars show means of the four samples. *, $P < 0.05$; **, $P < 0.001$. (G) BALB/c mice ($n = 8$) were infected with 10^3 *rop18-KO* parasites complemented with the indicated vectors, and the survival rates were monitored for 20 d. (B–G) Data are representative of two independent (B, C, E, and F) or cumulative percentages of two independent (D and G) experiments.

Published June 13, 2011

infection (Saeij et al., 2006, 2007). Subsequently, this effector molecule was shown to directly phosphorylate Stat3 and Stat6, and the N-terminal extension of ROP16 was demonstrated to play a key role in the interaction with the substrates (Yamamoto et al., 2009; Ogawa et al., 2010; Ong et al., 2010). Like ROP16, ROP18 exhibits an uncharacterized N-terminal extension (El Hajj et al., 2006).

To explore the function of the N terminus of ROP18, we first generated ROP18-deficient type I parasites and confirmed the in vivo significance of ROP18 in the type I parasite–mediated virulence. Complementation experiments showed that the N-terminal portion of ROP18 is required for the full recovery of virulence in *rop18-KO* parasites. A yeast two-hybrid screening and biochemical experiments found that the host factor ATF6β is a binding partner with the N-terminal extension of ROP18. This association led to a proteasome-dependent degradation of ATF6β in a kinase activity–dependent manner. Consistent with a defensive function of ATF6β against the parasite, ATF6β-deficient mice were generated and shown to be highly susceptible to *rop18-KO* but not WT parasites. Collectively, these results identified ATF6β as one of the host cellular factors targeted by ROP18 in the context of acute pathogenesis by the type I *T. gondii* strain.

RESULTS

The N terminus of ROP18 is involved in acute virulence in type I parasites

To determine whether ROP18 contributes to the high mortality rate of type I strains in mice, we disrupted the *ROP18* gene in the type I RH strain by reverse genetics and isolated several independent clones (Fig. 1, A and B). Northern blot analysis confirmed the absence of *ROP18* messenger RNAs in the clones (Fig. 1 C). The parasite lytic cycle as measured by plaque assay and intracellular growth on human foreskin fibroblasts (HFFs) was unaffected in these mutants as compared with WT parasites (Fig. S1, A and B). The recruitment of host organelles such as the mitochondria and ER around the PV was unaltered (unpublished data). We first challenged BALB/c mice with WT or *rop18-KO* parasites and monitored animal survival for 20 d. All mice infected with WT parasites died within 9 d. In contrast, mice infected with *rop18-KO* parasites showed a considerably lower mortality rate (Fig. 1 D). Luciferase-expressing WT or *rop18-KO* parasites were generated to visualize the in vivo parasite burden in BALB/c mice. A significantly stronger signal was detected in the ventral side of mice infected with WT parasites than those with *rop18-KO* parasites (Fig. 1 E). Moreover, the photon flux measurement during the course of infection increased notably faster and demonstrated a two log difference between WT and *rop18-KO* parasites at 7 d after infection (Fig. 1 F). Given the importance of the N-terminal extension for ROP16, we complemented *rop18-KO* parasites with full-length Flag-tagged (F) ROP18 (*ROP18_F* strain), the ROP18 mutant deleted in residues 147–164 of the N-terminal portion (*ΔN2-ROP18_F* strain), or the empty vector (*Empty vector* strain) and tested the recovery of the acute virulence phenotype (Fig. S2, A and B). Expression of ROP18_F fully restored acute virulence, whereas the *Empty vector* parasites exhibited an avirulent phenotype comparable with the parental *rop18-KO* parasites. The recovery of the virulence in *ΔN2-ROP18* parasites was only partial compared with the *ROP18_F* strain (Fig. 1 G). These data formally establish that ROP18 is a virulence factor of acute toxoplasmosis in type I strain and highlight the important contribution of the N-terminal extension of ROP18 for the full manifestation of the virulence phenotype.

Enhanced type I immune responses in mice infected with *rop18-KO* parasites

We next compared type I immune responses in the infected BALB/c mice because IFN-γ, mainly produced by Th1-polarized CD4 and CD8 T cells, plays a critical role in the control of acute toxoplasmosis (Subauste and Remington, 1991; Shirahata et al., 1994; Yap and Sher, 1999). 6 d after infection, CD4 and CD8 T cells from the spleens of mice demonstrating no abnormalities in appearance and no alteration in splenic cellularities and were tested for IFN-γ production by anti-CD3 treatment (Fig. S3, A–C). Compared with T cells from mice infected with WT parasites, CD4 and CD8 T cells from those infected with *rop18-KO* parasites displayed dramatically higher IFN-γ production in response to anti-CD3 (Fig. 2, A and B). To analyze antigen-specific IFN-γ production, we next compared the production from T cells stimulated with heat-killed *T. gondii* in the presence of DCs. Even in this condition, CD4 and CD8 T cells from mice infected with *rop18-KO* parasites produced higher concentrations of IFN-γ than those infected with WT parasites (Fig. 2, A and B). Collectively, these results show that ROP18 critically contributes to the suppression of the host type I immunity during infection with the virulent type I strain.

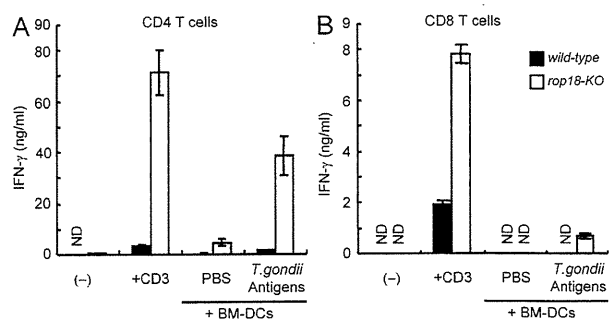

Figure 2. Enhanced IFN-γ production from T cells in mice infected with *rop18-KO* parasites. (A and B) CD4 (A) or CD8 (B) T cells from BALB/c ($n = 3$) mice were cultured in the presence of 5 µg/ml plate-bound anti-CD3 for 24 h or in the presence or absence of *T. gondii* antigen–pulsed BMDCs for 24 h. Concentration of IFN-γ in the culture supernatants was measured by ELISA. Indicated values are means ± SD of triplicates. Data are representative of three independent experiments. ND, not detected.

Published June 13, 2011

ROP18 interacts with ATF6β and mediates its degradation

The N-terminal extension of ROP16 interacts with the host factors Stat3/Stat6 (Yamamoto et al., 2009; Ogawa et al., 2010). Therefore, a yeast two-hybrid screening was undertaken to identify potential host partners interacting with the N-terminal portion of ROP18 (Nt-ROP18). ATF6β, a component of the ER membrane–bound transcription factor implicated in stress response, was found as the predominant hit, and its association with Nt-ROP18 was first confirmed in yeast cells (Fig. 3 A). Moreover, Nt-ROP18 and ATF6β failed to interact with SV40 large T antigen and p53 used as negative controls, respectively, demonstrating that Nt-ROP18 specifically associates with ATF6β in yeast (Fig. S4 A). To further assess the specificity of this interaction, we expressed Flag-tagged ROP18 lacking its signal peptide (Δ27-ROP18_F) or a larger N-terminal deletion of ROP18 (Δ240-ROP18_F) together with hemagglutinin (HA)-tagged ATF6β in mammalian 293T cells. Interestingly, we failed to detect an interaction between Δ27-ROP18_F and HA-ATF6β, but we noticed that overexpression of Δ27-ROP18_F but not Δ240-ROP18_F resulted in a dramatic reduction in the level of HA-ATF6β (Fig. 3 B). To determine whether parasite infection also caused a drop in HA-ATF6β levels, 293T cells expressing HA-ATF6β fused to CFP (with a self-cleavage signal [T2A] in between to produce the same level of both proteins) were similarly infected with WT or *rop18-KO* parasites (Fig. S4 B). The level of ATF6β protein was consistently reduced in cells infected with WT but not with *rop18-KO* parasites (Fig. 3 C). Moreover, Δ27-ROP18_F but not Δ240-ROP18_F decreased the ATF6β level in a dose-dependent fashion in dually transfected 293T cells (Fig. 3 D). ATF6β is a component of the ER stress response transcription factor that activates expression of genes harboring an unfolded protein response

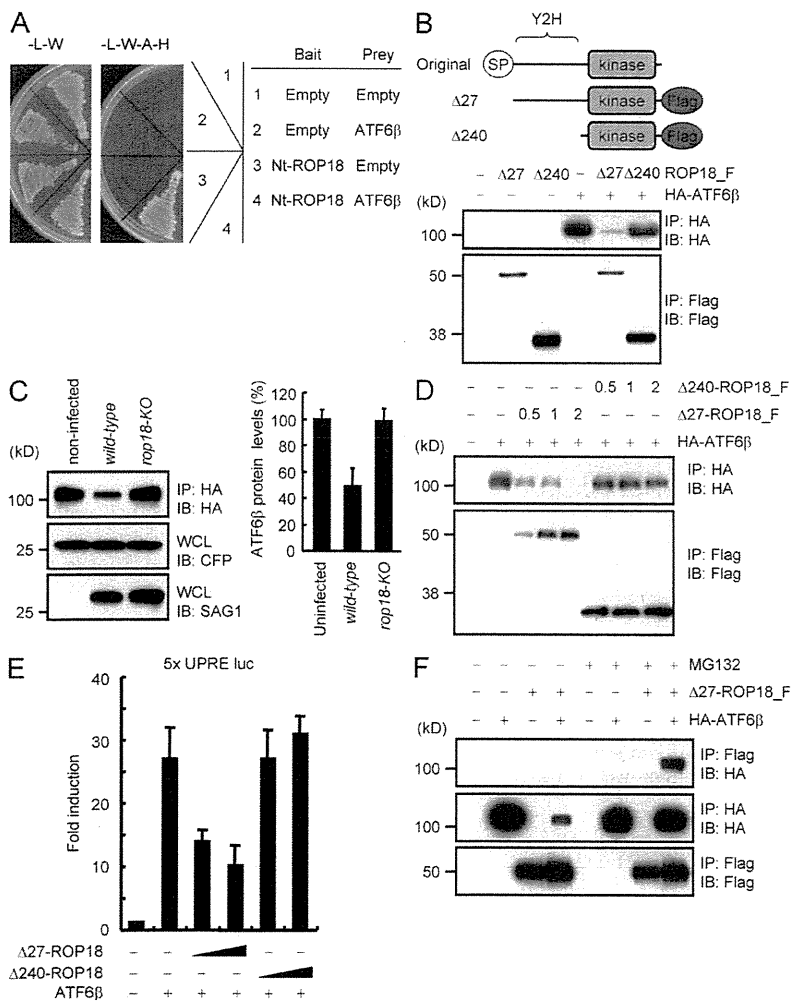

Figure 3. Identification of ATF6β as a ROP18-interacting protein. (A) Plasmids expressing Nt-ROP18 fused to the GAL4 DNA-binding domain or an empty vector were cotransfected with a plasmid expressing ATF6β fused to the GAL4 transactivation domain or an empty vector. Interactions were detected by the ability of cells to grow on medium lacking Ade, Trp, Leu, and His (-L-W-A-H). Growth of cells on plates lacking Trp and Leu (-L-W) was indicative of the efficiency of the transfection. (B) Lysates of 293T cells transiently cotransfected with 2 μg of the indicated Flag-tagged ROP18 and/or 2 μg HA-tagged ATF6β expression vectors were immunoprecipitated with the indicated antibodies and detected by Western blot with the indicated antibodies. The top images denote the structure of ROP18 variants used in this study. WT, original ROP18; SP, signal peptide; Y2H, the region used as the bait in the yeast two-hybrid screen. (C) The 293T cells transfected with 0.1 μg plasmids for tandem expression of HA-tagged ATF6β and T2A-CFP were infected with the indicated parasites at an MOI of 10. 24 h after infection, the cells were lysed and subjected to Western blot or immunoprecipitation (IP) with anti-HA (left). The expression levels of HA proteins were normalized against CFP (right). Error bars represent means ± the variation range of duplicates. IB, immunoblot; WCL, whole cell lysates. (D) Lysates of 293T cells transiently cotransfected with the indicated volumes of the Flag-tagged Δ27- or Δ240-ROP18 and/or 2 μg HA-tagged ATF6β expression vectors were immunoprecipitated with the indicated antibodies and detected by Western blot with the indicated antibodies. (E) 293T cells were transfected with the ATF6β-dependent luciferase reporter together with the indicated expression vectors. Luciferase activities were expressed as fold increases over the background levels shown by lysates prepared from mock-transfected cells. Error bars represent means ± SD of triplicates. (F) Lysates of 293T cells transiently cotransfected with 2 μg Flag-tagged ROP18 and/or 2 μg HA-tagged ATF6β expression vectors in the absence or presence of 10 μM MG132 for the last 12 h were immunoprecipitated with the indicated antibodies and detected by Western blot. (A–F) Data are representative of three (B and D–F) and two (A and C) independent experiments.

Published June 13, 2011

(UPR) element (UPRE) in their promoters (Wang et al., 2000; Yoshida et al., 2001). Overexpression of HA-ATF6β resulted in the activation of a UPRE-containing luciferase reporter in 293T cells; however, the coexpression of Δ27-ROP18_F but not Δ240-ROP18_F down-regulated the ATF6β-dependent activation in a dose-dependent manner (Fig. 3 E). To determine whether the ROP18-dependent decrease in ATF6β protein level is mediated by the proteasome, HA-ATF6β was coexpressed with Δ27-ROP18_F in the presence of the proteasome inhibitor MG132. Under this condition, the level of ATF6β was stabilized, and the interaction between Δ27-ROP18 and ATF6β could be monitored by coimmunoprecipitation (Fig. 3 F). Together, these data support the view that ROP18 associates with ATF6β and targets it to a proteasome-dependent degradation pathway.

The kinase activity of ROP18 is required for ATF6β degradation

ROP18 was previously shown to be a secreted active protein kinase in vitro and in vivo (Taylor et al., 2006; El Hajj et al., 2007). To assess whether the kinase activity of ROP18 plays a role in type I parasite–mediated pathogenicity, we complemented the *rop18-KO* parasites with WT (ROP18_F) or kinase-dead (KD; KD-ROP18_F) constructs (Fig. S2, B and C) and tested the virulence of the corresponding parasites in BALB/c mice (Fig. 4 A). Mice infected with *ROP18_F* resulted in 100% lethality within 10 d. In contrast, most of mice infected with *KD-ROP18_F* survived throughout the tested period. These results are consistent with a previous study, which reported that an avirulent type III strain expressing the *ROP18* but not the KD form of the type I strain can acquire virulence, pointing out the essential role of kinase activity of ROP18 for acute virulence (Taylor et al., 2006). To determine whether the kinase activity is involved in the ROP18-mediated degradation of ATF6β, mammalian expression vectors for KD-ROP18_F, ATF6β, and UPRE-containing luciferase reporter were cotransfected into 293T cells and followed by luciferase assays (Fig. 4 B). Overexpression of KD-ROP18_F failed to suppress ATF6β-mediated gene activation. Moreover, the

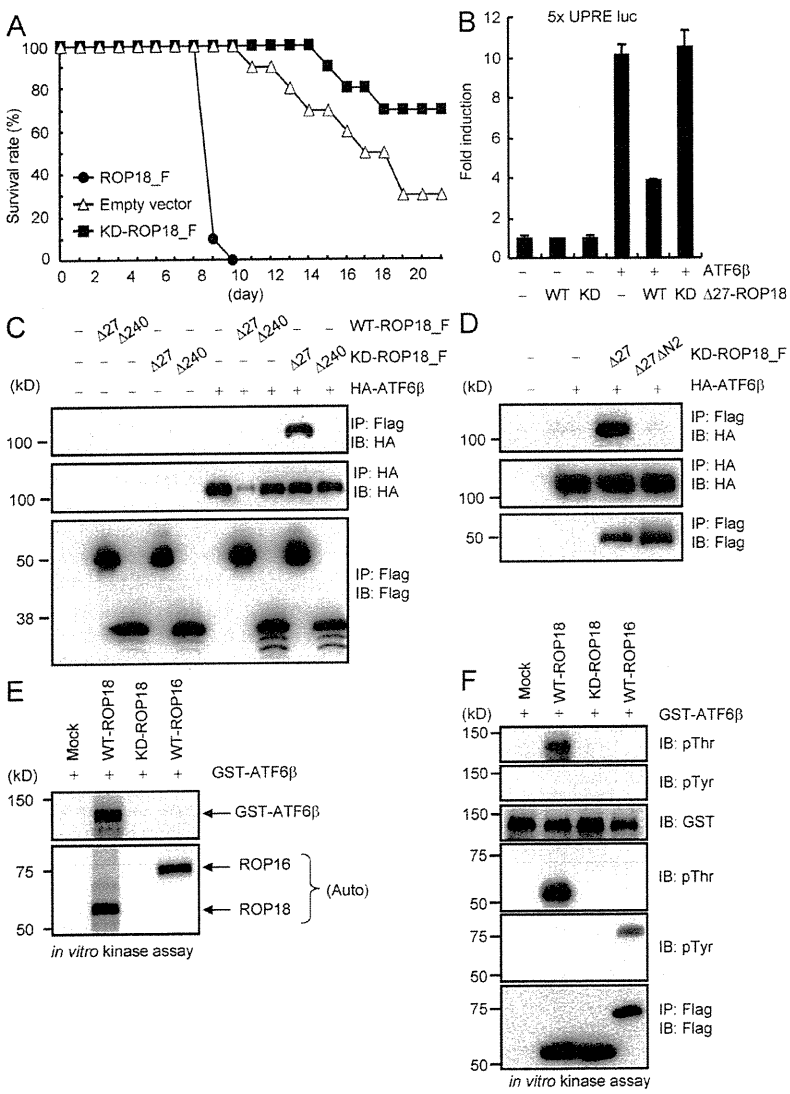

Figure 4. Essential role of ROP18 kinase activity in ATF6β degradation. (A) BALB/c mice ($n = 8$) were infected with 10^3 *rop18-KO* parasites complemented with the indicated vectors, and the survival rates were monitored for 20 d. (B) 293T cells were transfected with the ATF6β-dependent luciferase reporter together with the indicated expression vectors. Luciferase activities were expressed as fold increases over the background levels as shown by lysates prepared from mock-transfected cells. Error bars represent means ± SD of triplicates. (C and D) Lysates of 293T cells transiently cotransfected with 2 μg of the indicated Flag-tagged ROP18 and/or 2 μg of HA-tagged ATF6β expression vectors were immunoprecipitated with the indicated antibodies and detected by Western blot. (E and F) 293T cells were transiently transfected with Flag-tagged ROP18WT, ROP18KD, or ROP16WT. Cell lysates were immunoprecipitated with anti-Flag and subjected to an in vitro kinase reaction in the presence of GST-ATF6β. Proteins were separated on SDS-PAGE, followed by autoradiography (E) or Western blot (F) to analyze ATF6β phosphorylation or the autophosphorylation of ROP18 and ROP16. For the detection of phosphorylated or unphosphorylated GST-ATF6β and Flag-tagged proteins by Western blot, anti-pThr/anti-pTyr, anti-GST, and anti-Flag were used, respectively. IB, immunoblot; IP, immunoprecipitation. (A–F) Data are representative of three (B) or two (A and C–F) independent experiments.

Published June 13, 2011

ectopic expression of ROP18_F but not KD-ROP18_F led to HA-ATF6β degradation. KD-ROP18_F coprecipitated with ATF6β, as previously observed in the presence of MG132 (Figs. 3 F and 4 C). These results establish a connection between the kinase activity of ROP18 and ATF6β degradation. To examine which portion of the N terminus of ROP18 interacts with ATF6β, vectors expressing the KD versions Δ27- or Δ240-ROP18_F were introduced into 293T cells together with ATF6β. HA-ATF6β coprecipitated with Δ27-KD-ROP18_F but not with Δ240-KD-ROP18_F (Fig. 4 C). To refine the analysis, Δ27ΔN2-ROP18_F was cotransfected and shown to fail to coprecipitate with ATF6β (Fig. 4 D), indicating that the N-terminal 147–164 portion of ROP18 determines the binding to ATF6β. To challenge the possibility that ATF6β is a substrate for ROP18, we performed an in vitro kinase assay using recombinant glutathione *S*-transferase (GST)–tagged ATF6β as a substrate. Immunoprecipitates from 293T cells expressing Flag-tagged ROP18WT, ROP18KD, or ROP16WT were incubated with GST-ATF6β in the presence of radiolabeled ATP. Phosphorylation of GST-tagged ATF6β was detectable in the presence of ROP18WT but not with ROP18KD or ROP16WT (Fig. 4 E). To determine which amino acids on ATF6β are phosphorylated by ROP18, we relied on anti–phospho-Thr (anti-pThr), anti–pSer, and anti–pTyr. GST-tagged ATF6β was detected only in the presence of ROP18WT with anti-pThr, whereas anti-pSer and anti-pTyr gave no signal (Fig. 4 F and not depicted). In contrast, anti-pTyr detected autophosphorylation of ROP16WT (Fig. 4 F), correlating with the Tyr kinase activity of ROP16 (Yamamoto et al., 2009; Ong et al., 2010). Collectively, these results show that ROP18 phosphorylates at least one Thr residue on ATF6β, which leads to its degradation.

The C-terminal portion of ATF6β associates with ROP18

To characterize the region on ATF6β implicated in binding to ROP18, deletion mutants of ATF6β lacking both the transmembrane and the C-terminal portion (ΔCΔTM) or the C terminus alone (ΔC) were generated (Fig. 5 A). Activation of the UPRE-containing reporter by ΔCΔTM-ATF6β was unaffected by the presence of ROP18_F, even at high doses (Fig. 5 B). Moreover, KD-ROP18_F coprecipitated with the HA-tagged full-length ATF6β but not with the ΔC form (Fig. 5 C), suggesting that the C-terminal portion of ATF6β is implicated in the association with ROP18. Intriguingly, the family members of ATF6 proteins are anchored in the membrane of the ER with their C-terminal region predicted to localize in the lumen (Stirling and O'Hare, 2006). If this topology holds true for ATF6β, it would imply that ROP18 needs to gain access to ATF6β in the host ER. To examine whether ROP18 localizes to the ER, YFP-tagged ATF6β and T2A_CFP-tagged KD-ROP18 were bicistronically cloned and coexpressed with an ER-localized RFP in 293T cells (Fig. S5, A and B). Live microscopy revealed colocalization of ER-localized RFP and CFP-ROP18, suggesting that ROP18 is in close proximity with ER-resident proteins. The host ER has recently been reported to fuse with the PV membrane (PVM; Sinai et al., 1997; Goldszmid et al., 2009), and thus it is plausible that ER-localized ATF6β in the vicinity of PVMs might be targeted by ROP18. Indeed, when HFFs infected with parasites were analyzed by electron microscopy, PVMs not only associated with, but also appeared to directly fuse with the host ER (Fig. S5 C). These results indicate that the functional ROP18 kinase is necessary to trigger degradation of ATF6β and suggest that ROP18 might colocalize with ATF6β in the host ER or at the PVM.

Defensive function of ATF6β against infection of *rop18-KO* parasites

Given the correlation between the ability of ROP18 to induce ATF6β degradation and manifestation of virulence in type I parasites, we hypothesized that mice infected with *rop18-KO* parasites are resistant, at least in part, because of a protective effect dependent on ATF6β. To test this possibility under physiological conditions, we generated mice lacking the *Atf6β* gene (Fig. S6, A–C). Homozygous mice with the *Atf6β*-deleted allele were born at the expected Mendelian ratio and grew healthy in specific pathogen–free conditions, as previously reported for another line of ATF6β-deficient mice (Yamamoto et al., 2007). In terms of the cellularity of immune cells under unstimulated conditions, ATF6β-deficient mice behaved similarly to WT mice (unpublished data). When

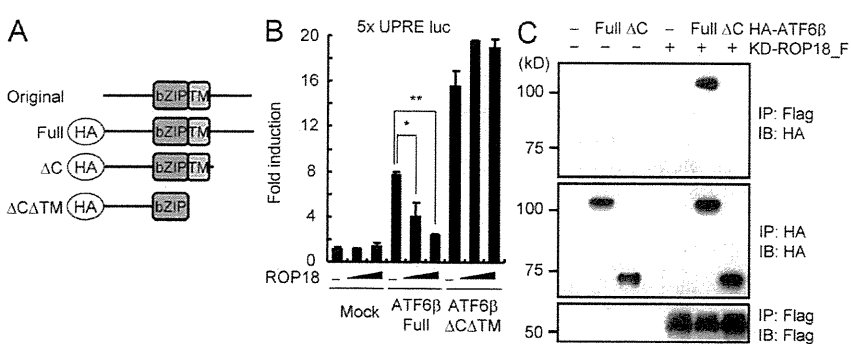

Figure 5. The C-terminal portion of ATF6β interacts with ROP18. (A) HA-tagged ATF6β variants. bZIP, basic Leu zipper; TM, transmembrane. (B) 293T cells were transfected with the ATF6β-dependent luciferase reporter together with the indicated expression vectors. Luciferase activities were expressed as fold increases over the background levels as shown by lysates prepared from mock-transfected cells. Error bars represent means ± the variation range of duplicates. *, $P < 0.03$; **, $P < 0.001$. (C) Lysates of 293T cells transiently cotransfected with 2 μg of the indicated Flag-tagged ROP18 and/or 2 μg of the indicated HA-tagged ATF6β expression vectors were immunoprecipitated with the indicated antibodies and detected by Western blot. IB, immunoblot; IP, immunoprecipitation. (B and C) Data are representative of three (C) or two (B) independent experiments.

Published June 13, 2011

challenged with parasites, ATF6β-deficient mice were more susceptible to *rop18-KO* parasites than WT mice (Fig. 6 A). In sharp contrast, the susceptibility of both genotypes of mice infected with WT parasites was comparable (Fig. S6 D). Moreover, ATF6β-deficient mice similarly succumbed to infection with complemented *rop18-KO* parasite lines (Fig. S6 E). The CTG strain was used as a natural *rop18-KO* parasite and shown to cause a higher mortality rate in ATF6β-deficient mice than in WT mice (Fig. S6 F). To follow more accurately the course of infection, WT and ATF6β-deficient mice were infected with 10^3 luciferase-expressing *rop18-KO* parasites, and the kinetics of infection were monitored by in vivo imaging. Marked increments of *rop18-KO* parasites were observed at days 5, 7, and 8 in ATF6β-deficient mice compared with WT mice (Fig. 6, B and C). To assess whether type I immune responses in ATF6β-deficient mice were affected, the T cell responses were examined at day 6 after infection with *rop18-KO* parasites. The cellularities after the parasite challenges were unchanged in WT and ATF6β-deficient mice (unpublished data). Under these conditions, a significantly reduced IFN-γ response to anti-CD3 was observed in CD8 T cells but not in CD4 T cells (Fig. 6 D). Next, we examined whether the defective IFN-γ production from ATF6β-deficient cells is intrinsic or extrinsic to CD8 T cells. WT DCs were infected with irradiated *rop18-KO* parasites in vitro, and then intraperitoneally injected into WT or ATF6β-deficient mice. 6 d after the injection, splenic CD4 and CD8 T cells were isolated and co-cultured with WT DCs noninfected or infected with *rop18-KO* parasites, and the supernatants were analyzed for IFN-γ production. Comparable IFN-γ production was observed in WT and ATF6β-deficient CD8 T cells, suggesting that the defective IFN-γ production in ATF6β-deficient CD8 T cells may be extrinsic to the T cells (Fig. 6 E). Next, to test whether APCs determine the phenotype, we collected splenic T cells from WT mice infected with *rop18-KO* parasites 6 d after infection and co-cultured with WT or ATF6β-deficient DCs noninfected or infected with *rop18-KO* parasites. We found that CD8 T cells with the infected ATF6β-deficient DCs produced significantly lower amounts of IFN-γ than those with WT DCs (Fig. 6 F). Thus, ATF6β in DCs is responsible for the CD8 T cell–mediated host defense against *rop18-KO* parasites.

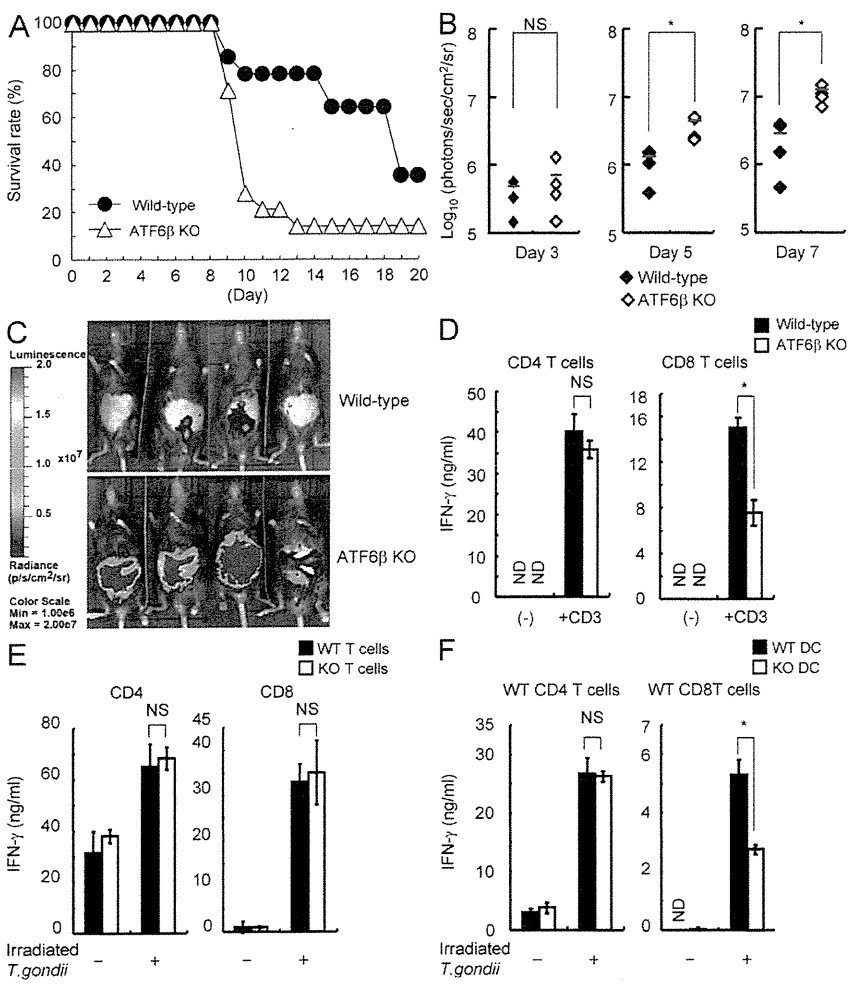

Figure 6. ATF6β functions as a host-defensive protein against *rop18-KO* parasites. (A) WT ($n = 14$) or ATF6β-deficient ($n = 14$) mice were infected with 10^3 *rop18-KO* parasites, and the survival rates were monitored for 20 d. (B) Total photon emission analysis from WT or ATF6β-deficient mice ($n = 4$) infected with 10^3 *rop18-KO* luciferase-expressing parasites at days 3, 5, or 7 after infection. Abdominal photon emission was assessed during a 60-s exposure. The red bars show means of the four samples. *, $P < 0.05$. (C) WT or ATF6β-deficient mice ($n = 4$) were infected with 10^3 *rop18-KO* luciferase-expressing parasites, and the progress of the infection was assessed by bioluminescence imaging at day 8 after infection. Color scales indicate photon emission during a 60-s exposure. (D) CD4 or CD8 T cells from WT or ATF6β-deficient mice ($n = 4$) were cultured in the presence of 5 μg/ml plate-bound anti-CD3 for 24 h. (E) WT DCs infected with irradiated *rop18-KO* parasites were injected into WT or ATF6β-deficient mice. 6 d after DC injection, CD4 or CD8 T cells purified from the spleens were restimulated with DCs uninfected or infected with *rop18-KO* parasites for 48 h. (F) CD4 or CD8 T cells purified from WT mice infected with *rop18-KO* parasites 6 d after infection were restimulated with WT or ATF6β-deficient DCs uninfected or infected with *rop18-KO* parasites for 48 h. (D–F) Concentration of IFN-γ in the culture supernatants was measured by ELISA. Indicated values are means ± SD of triplicates. *, $P < 0.05$. ND, not detected. (A–F) Data are representative of two (B–F) or a cumulative percentage of three (A) independent experiments.

Published June 13, 2011

ATF6β-independent response to the parasite infection

ΔN2-ROP18_F, which are insensitive to the ATF6β-mediated host response, moderately restored in vivo virulence (Fig. 1 G), suggesting that ATF6β-independent host responses may be functional to eliminate the parasites. Because ROP18 is shown to inactivate IRGs by the direct Thr phosphorylation (Fentress et al., 2010; Steinfeldt et al., 2010), we postulated the involvement of IRGs in the moderate host resistance in WT mice infected with *ΔN2-ROP18_F*. To assess whether ΔN2-ROP18 inactivates IRG, macrophages treated with IFN-γ were infected with *ROP18_F*, *ΔN2-ROP18_F*, *KD-ROP18_F*, or *EMPTY* parasites, and the interaction of an IRG Irgb6 with the ROP18 variants was examined by an immunoprecipitation assay (Fig. 7 A). ΔN2-ROP18_F as well as ROP18_F and KD-ROP18_F associated with Irgb6 in inflammatory macrophages. Next, we tested whether ΔN2-ROP18 mediates Thr phosphorylation on Irgb6 by an in vitro kinase assay. Immunoprecipitates of parasites expressing ΔN2-ROP18_F and ROP18_F but not KD-ROP18_F induced Thr phosphorylation of Myc-Irgb6-YFP but not Myc-YFP (Fig. 7 B and not depicted), indicating that activity of the IRG can be blocked by ΔN2-ROP18. Finally, to more carefully dissect contribution of the ATF6β-independent host response, ATF6β-deficient mice were infected with *rop18-KO* parasites complemented with ROP18 variants at a low dose (10^2 tachyzoites), and the parasite loads in the peritoneal cavities and IFN-γ production from splenic T cells were examined. Although the parasite number in mice infected with *Empty vector* was less than those in mice with *ROP18_F* or *ΔN2-ROP18_F* parasites at day 3 after infection, it was almost comparable at day 6. In contrast, the number of parasites in mice infected with *KD-ROP18_F* was consistently lower throughout the course of the experiment (Fig. 7 C). In terms of IFN-γ production, although the CD8 T cell–mediated production was unaltered, the production from CD4 T cells in mice infected with *ROP18_F* or *ΔN2-ROP18_F* was markedly reduced compared with that in mice with *KD-ROP18_F* or *Empty vector* (Fig. 7 D). Thus, these results suggest that the ATF6β-independent response regulates CD4 T cell–mediated IFN-γ production against *rop18-KO* parasites.

DISCUSSION

In this study, we provide the first genetic and biochemical evidence that the host cellular protein, ATF6β, is targeted for degradation by ROP18, a key virulence factor in *T. gondii*. ATF6β is a member of the ATF6-related family of transcription factors that have been shown to operate in the UPR (Yoshida et al., 2001; Yamamoto et al., 2007). Recently, UPR-related molecules such as XBP-1 in *Caenorhabditis elegans* or mammals and a plant ATF6-related molecule were shown to be involved in host

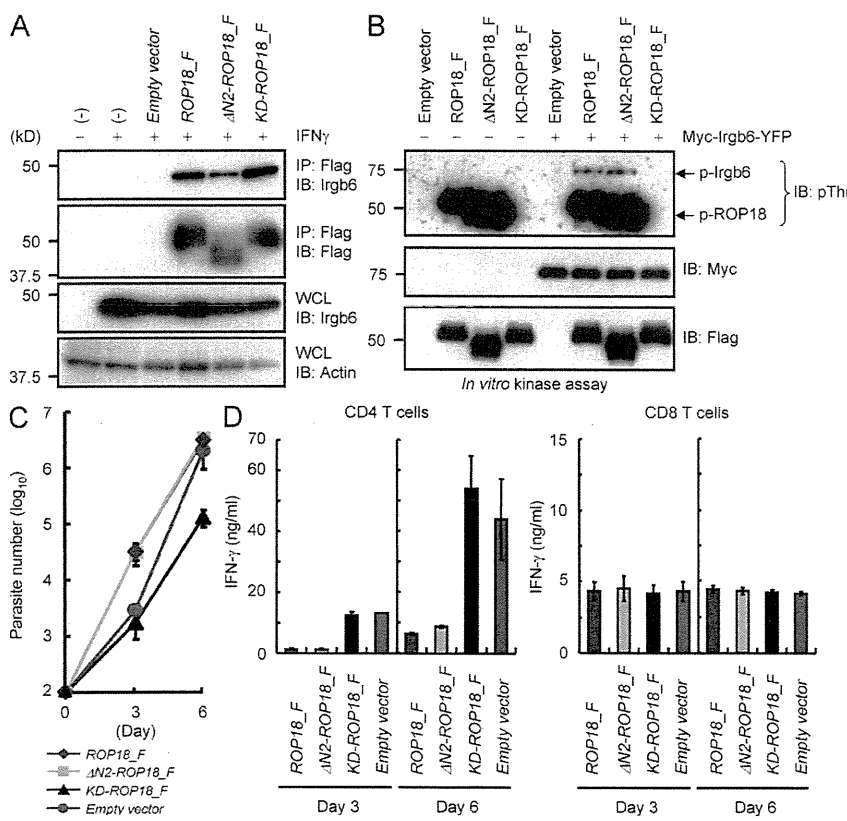

Figure 7. Parasite-induced ATF6β-independent host response. (A) Peritoneal macrophages treated with 30 ng/ml IFN-γ for 24 h were infected with the indicated parasites. Lysates of the infected cells were immunoprecipitated with anti-Flag and detected by Western blot with the indicated antibodies. IB, immunoblot; IP, immunoprecipitation; WCL, whole cell lysate. (B) 293T cells were transiently transfected with empty or Myc-tagged Irgb6-YFP vectors. Cell lysates were immunoprecipitated with anti-Myc and subjected to an in vitro kinase reaction in the presence of anti-Flag immunoprecipitates of the indicated parasites. Proteins were separated on SDS-PAGE, followed by Western blot to analyze Irgb6 phosphorylation or the autophosphorylation of ROP18. For detection of phosphorylated or unphosphorylated Myc-Irgb6-YFP and Flag-tagged proteins by Western blot, anti-pThr, anti-Myc, and anti-Flag were used, respectively. (C and D) ATF6β-deficient mice ($n = 3$) intraperitoneally infected with a dose of the indicated 10^2 parasites. Peritoneal fluids were collected at the indicated days after infection, and the parasite numbers were counted by plaque forming assays (C). CD4 or CD8 T cells from spleens of mice infected with the indicated parasites were cultured in the presence of 5 μg/ml plate-bound anti-CD3 for 24 h. Concentration of IFN-γ in the culture supernatants was measured by ELISA. Indicated values are means ± SD of triplicates. (A–D) Data are representative of two independent experiments.

Published June 13, 2011

defense against pathogens (Tateda et al., 2008; Martinon et al., 2010; Richardson et al., 2010). In this study, we report the protective effect of ATF6β against *rop18-KO* but not WT parasite infection. It remains to be determined whether ATF6β also participates in host defense against other pathogens and whether other ATF6 family members including ATF6α and Creb3 (also known as Luman) are targeted by ROP18 (Liang et al., 2006; Zhang and Kaufman, 2008).

Our data suggest that ATF6β deficiency in DCs rather than in T cells is responsible for the defective production of IFN-γ in CD8 T cells, yet a formal proof would require the conditional ablation of ATF6β in these cell types. Given that ATF6β acts as transcription factor, it will be important to determine which of the ATF6β-regulated genes mediate DC activation leading to CD8 T cell responses.

DCs treated with an inhibitor of the ER-associated degradation (ERAD) system were shown to fail to induce CD8 T cell response by cross-presentation (Goldszmid et al., 2009). The close association and possible fusion of host ER with the PV of *T. gondii* could cause an ER overload leading to ERAD activation (Sinai et al., 1997; Goldszmid et al., 2009). Interestingly, the ATF6 family members regulate the transcription of a subset of ERAD components (Wu et al., 2007), so it is conceivable that type I virulent *T. gondii* strains might target ATF6β in DCs (or other APCs such as macrophages) to down-regulate UPR-meditated host defense (Blanchard and Shastri, 2010). The data presented in this study are consistent with the previous findings that (part of) host ERs fuse with PVs during *T. gondii* infection (Goldszmid et al., 2009; Melo et al., 2010). However, studies showing that some ER-resident proteins colocalized with the PVMs do not constitute direct evidence for the host ER–PV fusion, and thus more in depth analysis is required to support this model.

ATF6β-deficient mice are highly susceptible to *rop18-KO* parasites with high parasite burdens possibly caused by defective IFN-γ responses of CD8 T cells. However, T cells from dying ATF6β-deficient mice (for instance, at days 9–10 after infection), in which the spleen was about to be autodigested and partly adhesive to other organs, secreted extremely high concentrations of IFN-γ even under nonstimulated conditions (unpublished data), which is indicative of an overreacting immune responses just before death. Thus, high susceptibility to the parasites might be primarily attributable to the excessive parasite proliferation and terminally dysregulated immune pathology.

Previous studies reported that ROP18-overexpressing parasites exhibited accelerated growth (Taylor et al., 2006; El Hajj et al., 2007). In contrast, the *rop18-KO* parasites showed normal intracellular growth in this study. It is plausible that overexpression of ROP18 impacts proliferation by acting on additional host cell substrates that are not essential to promote normal growth of *rop18-KO* parasites.

Expression of ΔN2-ROP18_F, which lacks the ATF6β-binding region, moderately restores the virulence of *rop18-KO* parasites. Because this ROP18 mutant does not associate with ATF6β, ATF6β-mediated host defense might be functional in *ΔN2-ROP18_F* parasite infection. Nevertheless, *ΔN2-ROP18_F* parasites are not avirulent, indicating the existence of an additional ROP18-mediated but ATF6β-independent virulence mechanism. ΔN2-ROP18_F lacks 17 aa in the N terminus of ROP18, which corresponds to helix 2 of the ROP5 N-terminal extension that is essential for its localization to the PV (Reese and Boothroyd, 2009). Similarly, ROP18 is injected into the host cytosol during invasion and is ultimately found at the PV (Boothroyd and Dubremetz, 2008). The *ΔN2-ROP18_F* strain might incapacitate ATF6β-independent innate immune responses, including IRG-mediated resistance which is operative soon after the parasite invasion (Hunn et al., 2008; Zhao et al., 2009; Khaminets et al., 2010). Indeed, ROP18 has recently been shown to target the member of IRGs, Irgb6 (Fentress et al., 2010; Steinfeldt et al., 2010). In this study, we characterized ATF6β-independent immune responses in ATF6β-deficient mice infected with *ΔN2-ROP18_F*, which inactivated Irgb6. Compared with infection of *EMPTY* or *KD-ROP18_F*, *ΔN2-ROP18_F* infection resulted in much reduced CD4 T cell–mediated IFN-γ production, suggesting that IRGs may be involved in activation of the ATF6β-independent CD4 T cell response. However, this assumption is contradictory to previous findings that the Stat1–IRG axis is not required for the development of Th1 immunity (Taylor et al., 2000; Collazo et al., 2001; Lieberman et al., 2004). This may be caused by strain-dependent differential host innate immune responses (Robben et al., 2004). Previous studies used type II parasites, whereas this study used type I parasites. IRG-deficient mice with high numbers of type II parasites are shown to culminate in higher concentrations of IL-12 in vitro and in vivo than that in WT mice, possibly leading to the development of apparently normal Th1 immunity that can compensate for the defect in the potential IRG-mediated CD4 T cell phenotype (Taylor et al., 2000; Collazo et al., 2001). Alternatively, the other ATF6β/IRG-independent ROP18-mediated effector mechanisms may suppress the CD4 T cell response. It is of interest in the future to revisit the potential involvement of IRGs in the development of CD4 T cell response using relatively immune-silent but IRGs-sensitive type I *rop18-KO* or type III parasites.

Despite the CD4 T cell–mediated IFN-γ production and the successful suppression of *rop18-KO* parasite (*Empty vector*) increment at the early stage after infection, ATF6β-deficient mice allowed the parasites to proliferate at the late stage and eventually succumbed. The CD8 T cell–mediated response is defective in ATF6β-deficient mice. Moreover, mice deficient in CD8 but not CD4 T cell functions are highly susceptible to acute toxoplasmosis (Casciotti et al., 2002; Combe et al., 2005; Lu et al., 2009). Therefore, even though the ATF6β-independent mechanism activates the CD4 T cell–mediated immunity that contributes to host resistance at early stages, it might be ultimately incompetent to counteract the acute parasite infection under condition of the defective CD8 T cell responses. In contrast, considering that the *rop18-KO* parasites (*Empty vector*) are not as virulent as the *ΔN2-ROP18_F* in WT mice, the ATF6β-independent CD4 T cell response

Published June 13, 2011

JEM

may considerably enhance host resistance under the normal CD8 T cell conditions. Previous studies established that interference with the innate function of Irgb6 is an important mechanism of ROP18-mediated virulence especially at an early stage after infection (Fentress et al., 2010; Steinfeldt et al., 2010). Furthermore, our study reveals that ROP18 also targets ATF6β-dependent CD8 T cell–mediated acquired immune responses that act at a later stage after infection. Thus, ROP18 may continue to disarm host immunity during the acute pathogenesis by targeting different host factors at each stage.

In conclusion, this study identifies ATF6β as a novel and unexpected substrate for ROP18. This finding nicely complements the recently published study to establish that the kinase activity of ROP18 is essential for the mortality phenotype and may be required for the suppression of both the ATF6β-dependent and -independent host defense mechanisms (Taylor et al., 2006). Interestingly, KD-ROP18_F expression in *rop18-KO* parasites appeared to reduce virulence. Because ROP18 belongs to the ROP2 subfamily consisting of >30 members including 17 active kinases (Peixoto et al., 2010), it is possible that expression of KD-ROP18 might have a dominant-negative effect, suppressing the action of other family members implicated in virulence. Whether other ROP2 subfamily members are important for the type I parasite–mediated virulence in concert with ROP18 should be examined in the future. Intriguingly, type II parasites are shown to be avirulent in spite of normal expression levels of ROP18. Given that ROP16 does not act positively in the virulence (Saeij et al., 2006), type II parasites might be defective in other ROP2 subfamily members.

In summary, ATF6β has been associated in this study for the first time with a resistance mechanism against an intracellular pathogen. ROP18, an effector molecule that constitutes the major virulence factor *T. gondii* type I strain, controls ATF6β degradation. In the future, the in vitro assay system based on the UPR-containing reporter may facilitate the development of a new pharmaceutical drug targeting ROP18 that can block acute toxoplasmosis.

MATERIALS AND METHODS

Cells, mice, and parasites. BALB/c and outbred CD1 ICR mice (6–8 wk old) were obtained from SLC. All animal experiments were conducted with the approval of the Animal Research Committee of the Graduate School of Medicine at Osaka University. RHΔhxgprt and its derivatives of *T. gondii* were maintained in Vero or HFFs by biweekly passage in RPMI (Nacalai Tesque) supplemented with 2% heat-inactivated FCS (JRH Biosciences), 100 U/ml penicillin, and 0.1 mg/ml streptomycin (Invitrogen). The CTG strain was provided by D. Sibley (Washington University School of Medicine, St. Louis, MO) and maintained in Vero cells in the RPMI media.

Reagents. Antibodies against *T. gondii* major surface antigen 1 (SAG1), anti-TGTP (Irgb6), anti-Myc, and HA probe were obtained from Santa Cruz Biotechnology, Inc. Anti-pTyr and anti-pThr were obtained from Cell Signaling Technology. Anti-Flag and anti-pSer were obtained from Sigma-Aldrich. Anti-ROP1 was provided by J.F. Dubremetz (Université de Montpellier 2, Montpellier, France). For indirect immunofluorescence, anti-HA rat antibody was obtained from Roche. MG132 was obtained from EMD.

Generation of RHΔhxgprt *T. gondii*–expressing OVA and a fusion protein of RFP and luciferase. To express luciferase, RFP, and OVA, we constructed a plasmid harboring p30-OVA and luciferase-RFP fusion proteins (pOVRFPluc). The luciferase and RFP fragments were obtained by PCR using primers OVA_F and OVA_R, with plasmid pGL3 as the template or primers RFP_F and RFP_R using pDsRed-express (Takara Bio Inc.) as the template, respectively. The information for all primers used in this study is listed in Table S1. The EcoRI–XhoI fragment of luciferase and the XhoI–PacI fragment of RFP were cloned into the EcoRI–PacI-digested sag1-ROP16HA-3UTR plasmids (Yamamoto et al., 2009). The NotI fragment of sag1-Luciferase/RFP-3UTR was cloned into the site of p30-OVA plasmids (a gift from D.S. Roos, University of Pennsylvania, Philadelphia, PA), leading to the generation of the OVRFPluc plasmid. 100 μg of the OVRFPluc plasmids was transfected with RHΔhxgprt parasites, and the stable transformants were selected in RPMI media containing 20 μM chloramphenicol (Nacalai Tesque), as p30-OVA plasmids contained a cassette for the chloramphenicol resistance gene (Pepper et al., 2004). RFP-positive parasites were selected by fluorescent microscopy and tested for in vitro and in vivo luciferase activity. Three clones were isolated, and we observed comparable in vitro growth and in vivo virulence to each other and the parental line. Whether the parasite line, which was used for generation of *rop18-KO* parasites, expresses OVA has not been tested in this study.

Generation of ROP18-deficient type I *T. gondii*. Genomic DNA containing the *ROP18* gene was isolated by PCR using primers R18KOLA_F and R18KOLA_R to generate a 5.0-kb-long fragment. Primers R18KOSA_F and R18KOSA_R generated a 1.0-kb fragment. The gene encoding *T. gondii ROP18* consists of a single exon. The targeting vector (pKO-ROP18) was constructed by replacing the entire coding sequence of *ROP18* with the *HXGPRT* gene expression cassette (p2855). Outside the targeting vector, a YFP expression vector was ligated using a NotI site for the negative selection of random integration. 100 μg of the targeting vector linearized by ScaI was transfected into tachyzoites of the normal RHΔhxgprt parental strain or OVRFPluc RHΔhxgprt parasites as previously described (Yamamoto et al., 2009). After 25 μg/ml mycophenolic acid (MPA; Sigma-Aldrich) and 25 μg/ml xanthine (Wako Chemicals USA) selection for 14 d, MPA/xanthine-resistant colonies were sorted using a FACSAria (BD) to isolate YFP-negative parasites. The MPA/xanthine-resistant and YFP-negative parasites were subjected to limiting dilution to isolate the clones. A total of 142 clones were selected and screened by PCR for detecting homologous recombinants using primers DHFRrc01 (from the DHFR promoter of the *HXGPRT* expression vector) and R18ex01 (genomic sequence outside the short fragment of the *ROP18* locus), to detect homologous recombinants. This resulted in the isolation of four clones using normal RHΔhxgprt parasites and two homologous recombinants using OVRFPluc RHΔhxgprt parasites. Subsequently, genomic DNA of WT and ROP18-deficient parasites was extracted and subjected to Southern blot analysis using a DNA probe, which was generated by PCR using primers SB_F and SB_R. Additionally, to confirm the disruption of the gene encoding ROP18, we analyzed total RNA from WT and *rop18-KO* parasites by Northern blot using a DNA probe, which was generated by PCR using primers NB_F and NB_R.

Mammalian expression plasmids. The C-terminal Flag-tagged fragments of ROP18 lacking the N-terminal signal peptide were amplified using primers R18frg2common_F and R18frg2common_R. The series of ROP18 variants were amplified using primers R18D27frg1_F for Δ27, R18D240frg1_F for Δ240, primers for Δ27ΔN2 described in Table S1, and the common primer using genomic DNA from the RH strain and were ligated into the BamHI and NotI sites of a pcDNA vector. The kinase-inactive ROP18 mutant containing point mutations was generated using the primers D394A_F and D394A_R, and expression plasmids were generated using a site-directed mutagenesis kit (Agilent Technologies). The sequences of all constructs were confirmed with a genetic analyzer (ABI PRISM; Applied Biosystems). Human ATF6β cDNA was amplified using primers ATF6β_full_R for Full, ATF6β_DC_R for ΔC, ATF6β_DCDTM_R for ΔCΔTM, and the common primer

Published June 13, 2011

ATF6β_common_F using human BM cDNA as the template and then ligated into the EcoRI and NotI sites of a pcDNA vector for the N-terminal HA-tagged proteins (Invitrogen). Murine Irgb6 cDNA was amplified using primers Irgb6_F and Irgb6_R using IFN-γ–treated mouse macrophage cDNA as the template and then ligated into the EcoRI and XhoI sites of a pcDNA vector for the N-terminal HA-tagged and C-terminal YFP-tagged proteins. To express HA-hATF6β and CFP bicistronically using a self-cleavage T2A peptide (Holst et al., 2006), an expression vector for HA-hATF6β_T2ACFP was generated by ligation with a pcDNA vector for the N-terminal HA and EcoRI–XhoI fragment of hATF6β, which was generated by PCR using primers ATF6β_common_F and ATF6β_full_XhoI_R. T2ACFP was generated by PCR using primers T2ACFP_R and T2ACFP_F using a CFP vector as the template. The expression vector for HA_hATF6β_YFP-T2ACFP_KDROP18_Flag was constructed by cloning the EcoRI–XhoI fragment of hATF6β. The SalI–SacI fragment of YFP was amplified using primers YFP_F and YFP_R, using a YFP vector as the template. The SacI–BamHI fragment of T2ACFP and the BamHI–NotI fragment of KD-ROP18-Flag were inserted into the EcoRI–NotI site of the pcDNA vector for the N-terminal HA tag. By placing the T2A peptide between HA-hATF6β (or HA-hATF6β-YFP) and CFP (or CFP-KD-ROP18-Flag), we obtained independent and reliable expression of both proteins. The ER-localizing RFP vector pDsRed2-ER was purchased from Takara Bio Inc.

Generation of transgenic parasites. To complement the *rop18-KO* parasites, we generated an N-terminal signal peptide–containing ROP18, capable of being processed in the parasite, by PCR using the primer ParasiteR18frg1_F for ROP18-Flag (ROP18_F) or KD-ROP18_F and expressed the ROP18-F proteins driven by the sag1 promoter containing a pyrimethamine resistant gene cassette in the *rop18-KO* strain (Yamamoto et al., 2009). ΔN2-ROP18 lacking residues 147–164 of the N-terminal portion was generated by ligation of two fragments: one from the EcoRI–NotI fragment of ROP18_F and the other generated using primers ParasiteR18frg1F, DN2(ΔHX2)_F, and DN2(ΔHX2)_R. We generated this vector by digesting the pyrimethamine resistance cassette of the p2854 plasmid with NotI and XhoI and ligated this into a Klenow-treated pBluescript sag1-ROP18_F vector. A series of ROP18_F vectors or the empty p2854 vector for the generation of the *Empty vector* strain were transfected into tachyzoites of the *rop18-KO* parasites. We selected for parasites stably expressing the complemented ROP18_F constructs using 3 μM pyrimethamine (Sigma-Aldrich) selection and subjected these to limiting dilution as described previously (Yamamoto et al., 2009).

Generation of ATF6β-deficient mice. The *Atf6β* gene was isolated from genomic DNA extracted from embryonic stem cells (V6.5) by PCR using LA Taq (Takara Bio Inc.). The targeting vector (pKOATF6β) was constructed by replacing a 3.0-kb fragment encoding the exons of ATF6β with a neomycin-resistance gene cassette (*neo*) and a herpes simplex virus thymidine kinase gene driven by the PGK promoter, for negative selection. Genomic DNA containing the murine *Atf6β* gene was isolated by PCR amplification using primers ATF6βKO_LA_F and ATF6βKO_LA_R to generate a 5.0-kb fragment or primers ATF6βKO_SA_F and ATF6βKO_SA_R to generate a shorter 1.0-kb fragment. After the targeting vector was transfected into embryonic stem cells, colonies resistant to both G418 and ganciclovir were selected and screened by PCR and Southern blotting. Homologous recombinants were microinjected into C57BL/6 female mice, and heterozygous F1 progenies were intercrossed to obtain ATF6β-deficient mice. ATF6β-deficient mice and their WT littermates from these intercrosses were used for experiments.

Yeast two-hybrid analysis. Yeast two-hybrid screening was performed as described with the Matchmaker two-hybrid system (Takara Bio Inc.). For construction of the bait plasmid, the cDNA fragment coding the N-terminal portion (aa 35–235) of ROP18 was amplified using primers ROP18Y2H_F and ROP18Y2H_R and cloned in frame into the GAL4 DNA-binding domain of pGBKT7. Yeast strain AH109 was transformed with the bait plasmid plus the human BM Mate & Plate cDNA library (Takara Bio Inc.). After the screening of 10^7 clones, we finally obtained 10 positive clones and recovered the pGAD library from individual clones and expanded in *Escherichia coli*. The inserted cDNA was sequenced and characterized with the BLAST program, resulting in the identification of ATF6β (nine clones) and HLA-DPA1 (one clone). Because the number of positive clones of ATF6β was much greater than that of HLA-DPA1 and because HLA-DPA1 was difficult to be linked to the mouse homologue correctly compared with ATF6β, we selected ATF6β in the following study.

Luciferase reporter assay. The 5× UPRE luciferase reporter was generated by the synthesis of a 312-bp fragment containing five tandem ATF6 binding sites (Invitrogen), with the MluI–SalI fragment inserted into the MluI–XhoI site of the pGL3 luciferase reporter as described previously (Wu et al., 2007; Yamamoto et al., 2007). The reporter plasmids were transiently cotransfected into 293T cells with the control *Renilla* luciferase expression vectors using Lipofectamine 2000 reagent (Invitrogen). Luciferase activities of total cell lysates were measured using the Dual-Luciferase Reporter Assay System (Promega) as described previously (Yamamoto et al., 2006).

Statistical analysis. The unpaired Student's *t* test was used to determine statistical significance among experimental data.

Measurement of IFN-γ by ELISA. CD4 and CD8 T cells were obtained by positive selection using anti-CD4 (L3T4) and anti-CD8a (Ly-2) magnetic beads (Miltenyi Biotech) from splenocytes of mice at day 6 after infection with parasites and cultured for 24 h in 96-well plates (10^5 cells per well) precoated with 5 μg/ml anti-CD3 or preincubated with 10^5 BM-derived DCs (BMDCs) pulsed with heat-killed *T. gondii* antigens, which were prepared by incubation of 10^7 parasites at 56°C for 1 h. For the generation of BMDCs, BM cells were isolated from femurs and cultured with RPMI 1640 supplemented with 10% fetal bovine serum and 10 ng/ml GM-CSF (PeproTech) with medium replaced every 2 d. Concentration of IFN-γ in the culture supernatant was measured by ELISA according to the manufacturer's instructions (R&D Systems), as described previously (Yamamoto et al., 2003).

Western blot analysis and immunoprecipitation. The 293T cells and parasites were lysed in a lysis buffer (1% Nonidet P-40, 150 mM NaCl, and 20 mM Tris-HCl, pH 7.5) containing a protease inhibitor cocktail (Roche). The cell lysates were separated by SDS-PAGE and transferred to polyvinylidene fluoride membranes. For immunoprecipitation, cell lysates were precleared with protein G–Sepharose (GE Healthcare) for 2 h and then incubated with protein G–Sepharose containing 1.0 μg of the indicated antibodies for 12 h with rotation at 4°C. The immunoprecipitants were washed four times with lysis buffer and eluted by boiling with Laemmli sample buffer. The eluates were separated by SDS-PAGE, transferred to polyvinylidene fluoride membranes, and subjected to Western blot analysis as described previously (Yamamoto et al., 2004).

Flow cytometric analysis. 2×10^6 splenocytes were stained with PE-conjugated anti-B220, -CD8, or -CD11c, FITC-conjugated anti-CD3ε or -CD4, and APC-conjugated anti-Gr1. Stained cells were analyzed on a FACSCantoII (BD) and using FlowJo Software (Tree Star).

Microscopic analysis. The 293T cells were transfected with 2 μg of expression vectors for HA_ATF6β_YFP-T2ACFP–tagged KDROP18_Flag or ER-DsRed. At 24 h after transfection, cells were analyzed using a fluorescence microscope (IX71; Olympus).

Immunofluorescence analysis. HFF cells infected with parasites were fixed for 8 min in PBS containing 4% paraformaldehyde (PFA)/0.05% glutaraldehyde. Cells were permeabilized with PBS containing 0.2% Triton X-100 (PBS/TX) and then blocked with 2% BSA in PBS/TX. Subsequently, cells were incubated with anti-Rop1 rabbit antibody (1:200) and anti-Flag mouse

Published June 13, 2011

antibody (1:6,000; Sigma-Aldrich) for 1 h at room temperature, followed by incubation with Alexa Fluor 488–conjugated goat anti–rabbit IgG antibody (Invitrogen) and Alexa Fluor 594–conjugated goat anti–mouse IgG antibody (Invitrogen) for 45 min at room temperature in the dark. Finally, the immunostained cells were mounted with Fluoromount-G (SouthernBiotech) on glass slides and analyzed using a fluorescence microscope (Axioskop 2; Carl Zeiss) equipped with a color charge-coupled device camera (Axiocam HR; Carl Zeiss).

Plaque assay. The WT and *rop18-KO* parasites were used to infect monolayers of HFFs seeded in 24-well plates. After incubation for 8–9 d at 37°C, cells were fixed with 4% PFA and 0.05% glutaraldehyde in PBS, followed by staining with Giemsa for 10 min.

Assessment of intracellular growth. Host cells seeded on 24-well immunofluorescence assay plates were inoculated with freshly released WT or *rop18-KO* parasites. At 24 h after infection, parasites were fixed with 4% PFA. Immunofluorescence assays were performed using α-TgGAP45 antibody, and parasites were counted on at least 100 vacuoles for each strain.

Electron microscopy analysis. Monolayers of HFFs were infected with *rop18-KO* parasites. Samples were collected at 4 h after infection and processed for electron microscopy using routine techniques. In brief, parasite pellets were fixed in 2.5% glutaraldehyde in 0.1 M phosphate buffer, post-fixed in osmium tetroxide, dehydrated in ethanol, and treated with propylene oxide before embedding in Spurr's epoxy resin. Thin sections were stained with uranyl acetate and lead citrate before examination with an electron microscope (1200EX; JEOL).

In vivo imaging analysis. Mice were intraperitoneally infected with 10^3 freshly egressed tachyzoites resuspended in 100 µl PBS, with assessment of bioluminescence performed on the indicated days after infection. For the detection of bioluminescence emission, mice were intraperitoneally injected with 3 mg D-luciferin in 200 µl PBS (Promega), maintained for 5 min to allow for adequate dissemination of luciferin, and subsequently anaesthetized with isoflurane (Dainippon Sumitomo Pharma). At 10 min after injection of D-luciferin, photonic emissions were detected using an in vivo imaging system (IVIS 100; Xenogen) and Living image software (Xenogen).

Recombinant ATF6β purification. GST-tagged ATF6β cDNA was subcloned into pFAST-Bac (Invitrogen) for expression in Sf9 insect cells. Proteins were purified in accordance with the manufacturer's instruction as described previously (Yamamoto et al., 2006).

In vitro kinase assay. 5×10^6 293T cells (6-cm dish) were transiently transfected with a total of 4 µg of either empty vector or the indicated plasmids (4 µg of Flag-tagged ROP18WT, ROP18KD, or ROP16WT), using Lipofectamine 2000 as specified by the manufacturer. Cells were harvested 24 h after transfection, lysed, and then immunoprecipitated with protein G–Sepharose together with 1.0 µg anti-Flag M2 mAb (Sigma-Aldrich) for 12 h by rotation. The beads were washed four times with lysis buffer and another three times with kinase assay buffer (30 mM MOPS, pH 7.5, 50 mM NaCl, 10% glycerol, 10 mM $MgCl_2$, and 10 mM $MnCl_2$). The immunoprecipitates were incubated with 1 µg GST-ATF6β and 10 mCi γ-[^{32}P]ATP (GE Healthcare) or 5 µM cold ATP (Wako Chemicals USA) to phosphorylate GST-ATF6β, ROP18WT, ROP18KD, or ROP16WT at 30°C for 30 min. In the experiments for Fig. 7 B, immunoprecipitates of the parasites complemented with the ROP18 variants, which were prepared by immunoprecipitation of the parasite lysates by anti-Flag, were incubated with anti-myc immunoprecipitates of 293T cells transfected with control- or Myc-tagged Irgb6-YFP fusion vectors in the presence with 5 µM cold ATP in the kinase reaction buffer at 30°C for 30 min with gentle agitation. Kinase reactions were stopped by the addition of Laemmli sample buffer and were separated on a 5–20% polyacrylamide gradient gel. For radioactive samples, gel was detained, dried, and exposed to x-ray film. For cold samples, gel was detained and subjected to Western blot to detect unphosphorylated or phospho-GST–tagged ATF6β and Flag-tagged ROP18WT, ROP18KD, or ROP16WT by anti-GST, anti-pThr, anti-pSer, anti-pTyr, and anti-Flag, respectively.

Immunological experiments. To assess the phenotype in T cells (Fig. 6 E), DCs were generated from BMs of two WT mice cultured in GM-CSF. 2×10^7 DCs were collected at day 6 after cultivation and infected with irradiated *rop18-KO* parasites at multiplicity of infection (MOI) = 1 for 12 h. The cells were collected at 1,100 rpm and extensively washed with PBS three times at 4°C. 1,000,000 DCs were intraperitoneally injected into the littermates of WT or ATF6β-deficient mice ($n = 2$ for each group; $n = 4$ total for two independent experiments). 6 d after injection, CD4 or CD8 T cells were isolated by the positive selection of splenic T cells. The T cells (10^5 cells) were co-cultured with WT DCs (5×10^4 cells), which were freshly isolated from the littermate WT mouse and cultivated for 6 d in the presence of GM-CSF and uninfected or infected with irradiated *rop18-KO* parasites for 12 h at MOI = 1 for 48 h. The supernatants were collected and tested for ELISA to measure the IFN-γ concentration.

To analyze the phenotype of DCs for the ability of IFN-γ production from T cells (Fig. 6 F), CD4 and CD8 T cells were isolated from WT mice infected with 10^3 *rop18-KO* parasites 6 d after the infection. The T cells (10^5 cells) were co-cultured with DCs (5×10^4 cells), which were freshly isolated from the littermate WT or ATF6β-deficient mice ($n = 2$ for each group; $n = 4$ total for two independent experiments), and cultivated for 6 d in the presence of GM-CSF and uninfected or infected with irradiated *rop18-KO* parasites for 12 h at MOI = 1 for 48 h. The supernatants were collected and tested for ELISA to measure the IFN-γ concentration.

Quantification of parasite loads. The parasites in the peritoneal cavities were enumerated as described previously (Robben et al., 2005). In brief, total peritoneal contents were collected by injection of 5 ml of FCS-free RPMI into the peritoneal cavities of infected mice. Aliquots of the recovered fluids were added onto confluent monolayer of mouse embryonic fibroblasts in 96-well culture plates with 10-times serial dilutions from 10^0 to 10^5 and 4 wells of each dilution. 4 d after infection, the numbers of plaques were counted to calculate the total parasite numbers in the original peritoneal cavities.

Online supplemental material. Fig. S1 shows parasitological analysis of *rop18-KO* type I *T. gondii*. Fig. S2 demonstrates complementation of *rop18-KO* parasites by various ROP18 mutants. Fig. S3 exhibits splenic cellularity in mice infected with WT or *rop18-KO* parasites. Fig. S4 shows specific interaction of Nt-ROP18 with ATF6β in yeasts and similar infection levels between WT and *rop18-KO* parasites in 293T cells. Fig. S5 demonstrates ER localization of ROP18 and PVM–ER fusion. Fig. S6 describes the strategy for generation of ATF6β-deficient mice and shows comparable susceptibility in WT or ATF6β-deficient mice infected with WT *T. gondii*. Table S1 provides a list of the primers used in this study. Online supplemental material is available at http://www.jem.org/cgi/content/full/jem.20101660/DC1.

We thank C. Hidaka and M. Yasuda for excellent secretarial assistance, Y. Magota for technical assistance, and members of K. Takeda's laboratory for discussions. We are grateful to W. Daher for technical assistance and stimulating discussions. We also thank Professor D. Sibley for providing the CTG strain.

This work was supported by grants from the Ministry of Education, Culture, Sports, Science and Technology, the Strategic International Cooperative Program (Research Exchange Type), the Japan Science and Technology Agency, the Takeda Science Foundation, the Kanae Foundation for the Promotion of Medical Science, the Cell Science Research Foundation, the Ichiro Kanehara Foundation, the Kato Memorial Bioscience Foundation, and the Uehara Memorial Foundation. C. Mueller is supported by the Japanese-Swiss Science and Technology Program.

The authors have no conflicting financial interests to declare.

Submitted: 11 August 2010
Accepted: 23 May 2011